# A MECHANISTIC MODEL TO STUDY THE KINETICS AND TOXICITY OF SALICYLIC ACID IN THE KIDNEY OF FOUR VIRTUAL INDIVIDUALS


## Author names and affiliations

Julia Pletz[1], Terry J Allen[2], Judith C Madden[1], Mark TD Cronin[1], Steven D Webb[2,3]

[1] School of Pharmacy and Biomolecular Sciences, Liverpool John Moores University, Byrom Street, Liverpool L3 3AF, England

[2] Department of Applied Mathematics, Liverpool John Moores University, Byrom Street, Liverpool L3 3AF, England

[3] Syngenta, Jealott's Hill, Bracknell, Berkshire RG42 6EY, England

## ORCID IDs:

Julia Pletz: 0000-0002-7878-9668

Mark Cronin: 0000-0002-6207-4158

Judith Madden: 0000-0001-6142-5860

## Address and email of corresponding author

Julia Pletz, email: julia.pletz@yahoo.co.uk

**Keywords**

Mechanistic model, mathematical modelling, kidney toxicity, IVIVE, PBPK, PBK aspirin

**Abstract**

In comparison to liver toxicology, little is known about mechanisms of adverse effects in the kidney and only limited computational models exist to investigate nephrotoxicity. However, the kidney is a major target for toxicity by pharmaceuticals and environmental pollutants. Accumulation is known to play an important role in certain nephrotoxicity pathways. Therefore, physiologically-based kinetic (PBK) and mechanistic models are considered to offer valuable insights into mechanisms of nephrotoxicity. This study addresses the growing attention given to exposure-based and toxicokinetics-driven toxicity which has resulted in increasing recent application of PBK modelling. This research presents the development of a novel mechanistic kidney model embedded in a PBK model parameterised for aspirin and salicylic acid. It is set-up to study a combination of young/healthy individuals as well as the elderly, with three exposure scenarios simulating real renal exposure. Key challenges in this endeavour revolve around limited data available in the public literature and uncertainties related to scaling *in vitro* data to an *in vivo* setting. Results show that at a low, chronic therapeutic dose the predicted proximal tubular cell concentrations in all considered population groups are below the hypothesised toxicity threshold of 0.09 mM. Sensitivity analyses indicate that at both higher dose scenarios, active transporter activity has the most impact on predicted proximal tubular cell concentrations and therefore individual transporter expression may be key indicators of cellular toxicity.

## 1. Introduction

The kidney is a major target of drug-induced toxicity, particularly in vulnerable individuals such as patients who are critically ill and/or have chronic kidney disease (Mehta et al., 2004; Uchino et al., 2005; Zhang et al., 2005). The associated costs of chronic kidney disease (CKD) constitute a major and increasing challenge for national health care systems worldwide, with expenditures in England reaching £1.45 billion in 2009 and taking up close to 30% of general medical care costs in the U.S. in 2011 (Kerr et al., 2012; Collins et al., 2015; Eriksson et al., 2016). Whilst some of the pharmaceuticals responsible for nephrotoxicity have been on the market for decades, a detailed understanding of the toxicity pathways of most drugs is lacking (Pletz et al., 2018).

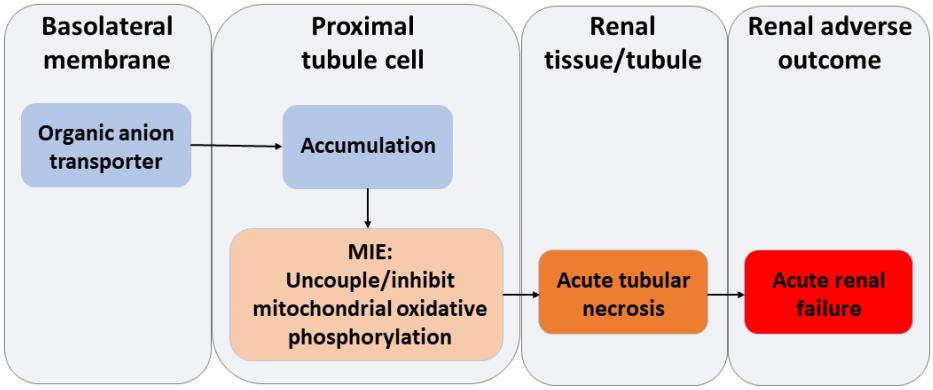


Figure 1: Summary of a proposed AOP for the nephrotoxicity of NSAIDs via the uncoupling/inhibition of mitochondrial oxidative phosphorylation (adapted with permission from Drewe and Surfraz, 2015)

It has been known for many years that therapeutic concentrations of salicylic acid (SA) in serum of 0.5 to 2.2 mM are high enough to induce mitochondrial swelling if the cytosolic concentration of an exposed cell is at the same level as the plasma concentration (You, 1983). SA is the major metabolite of the NSAID aspirin (acetyl salicylic acid; ASA). Despite the importance of mitochondrial dysfunction in renal disease (You, 1983; Ishimoto and Inagi, 2016; Eirin et al., 2017; Guo et al., 2018), including when elicited by NSAIDs (see Figure 1), a quantitative

evaluation of the concentration reached in proximal tubular cells at therapeutic and toxic exposures is still lacking. Such a quantitative assessment can be achieved with mechanistic models which use mathematical equations – typically ordinary differential equations (ODEs) – to reflect causal mechanisms driving input-output behaviours of biological systems (Oates and Mukherjee, 2012; Baker et al., 2018). These would add clarity to nephrotoxic effects observed in individuals at different dosing levels.

Most of the early mechanistic renal models (Tang-Liu et al., 1983; Hall and Rowland, 1984; Komiya, 1986, 1987; Mayer et al., 1988) derive quantitative relationships between renal clearance and urine flow, renal reabsorption, glomerular filtration and protein binding in various species and for a selection of substances, without compartmentalising the kidney. Russel et al. (1987a; b) and Katayama et al. (1990) differentiate between renal blood, tissue and tubular compartments. Felmlee et al. (2010, 2013) generated a universal mechanistic model to predict renal clearance driven by active secretion, active reabsorption or both of these processes. The authors separate a proximal tubule from a distal tubule compartment, in addition to including a renal blood and urine compartment.

Two of the most sophisticated mechanistic models to predict kinetics of chemicals in the kidney are reported by Neuhoff et al. (2013) and Huang and Isoherranen (2018). The structure of their models represents a nephron divided into segments illustrating the glomerulus, proximal and distal tubules, loop of Henle and collecting ducts. Each segment contains three compartments, characterising the cellular mass, blood space and tubular fluid. Both models predict renal elimination by accounting for active and passive reabsorption, active and passive secretion, glomerular filtration and renal metabolism. In both models, ODEs describe the movement of a compound between compartments so that the concentration of a substance can be quantified in each compartment. However, the model developed by Neuhoff et al. (2013) is embedded in

the commercial Simcyp® Simulator software and details of the ODEs are not publicly available. Applications of this model are reported (Hsu et al., 2014; Posada et al., 2015; Burt et al., 2016; Emami Riedmaier et al., 2016; Scotcher et al., 2017; Hsueh et al., 2018). The model generated by Huang and Isoherranen (2018) predicts drug renal clearance considering *in vitro* permeability, unbound filtration, active tubular secretion and pH dependent bidirectional passive diffusion. It is validated with data from 46 drugs.

In summary, there are limited computational models which quantify concentration-time profiles of substances in toxicologically relevant segments of the human kidney. To date, a publicly available kidney model which is embedded in a PBK model and has been tested for a sensitive population is lacking.

The aim of this study is to develop a mechanistic model of renal kinetics with specific reference to SA. Specific objectives include:

i. Incorporation of a sub-compartment mechanistic kidney model into a previously developed PBK platform in order to validate it with full-body kinetic data.
ii. Investigation into whether a quantitative relationship may be established between therapeutic doses of SA, predicted proximal tubular cell concentrations in young and elderly virtual individuals and toxicity events in proximal tubular cells.

## 2. Methods

### 2.1 Development of the model

A mechanistic model of the kidney was created using the SimBiology® desktop (version 5.8.1), an app provided by MATLAB®, version R2018b. The ODEs created in SimBiology are solved using the Matlab solver *ode15s* which integrates the system of stiff differential equations

(MathWorks, 2019). A principal assumption of the model is that compartments are well-stirred, which implies instantaneous and homogenous distribution of a compound within a compartment.

### 2.1.1 Structure and compartment volumes

As the nephron is the functional unit of a kidney, we assume that the core element of the kidney submodel is that of a nephron, connecting to a collecting duct. In the scientific literature, the latter is not considered part of the nephron (Fenton and Praetorius, 2015). The main components of a nephron include the glomerulus, proximal tubules, loop of Henle and distal tubules as shown in Figure 2. In a human kidney, 85% of the nephrons are predominantly located in the cortex, the outer region of the kidney, with short loops of Henle reaching the outer medulla (Feher, 2017). The remaining 15% are juxtamedullary nephrons which originate close to the corticomedullary boundary with long loops of Henle extending into the inner medulla (Fenton and Praetorius, 2015; Feher, 2017). Figure 2 shows a longitudinal cross-section of the kidney depicting key anatomic structures including the cortex and medulla.

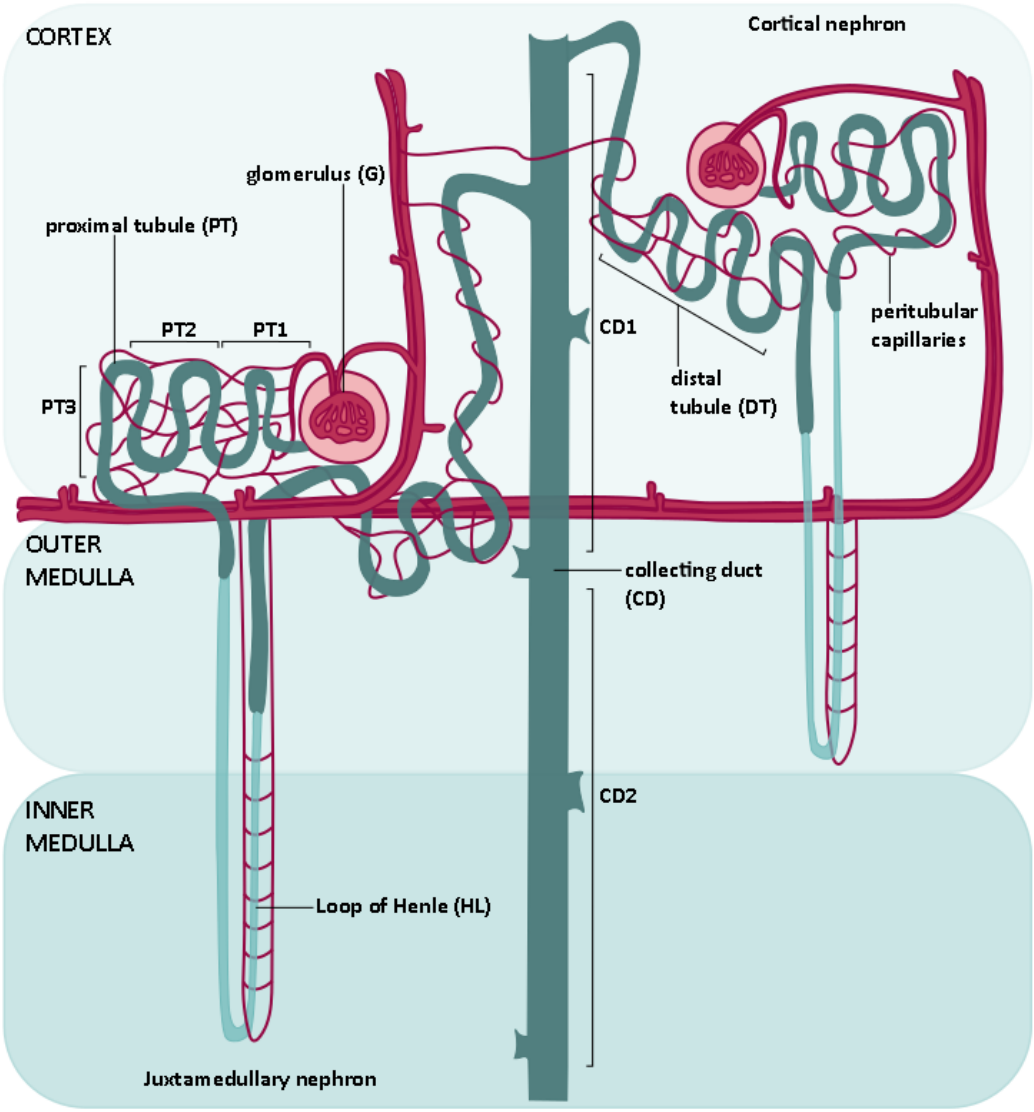


Figure 2: A schematic diagram of the structure of nephrons and their cortical and juxtamedullary locations relevant for the development of a mechanistic model (adapted with permission from Feher, 2017). The main components of the mechanistic model developed here are the glomerulus (G), proximal tubules divided into three sections (PT1-3), loop of Henle (HL), distal tubules (DT) and collecting ducts divided into two sections (CD1-2).

A substance reaches the nephrons via arterial blood vessels, so-called afferent arterioles which connect to the glomerulus where approximately 120 mL of water along with small, unbound substances are filtered per minute into the glomerular space. From there, the filtrate flows through the proximal tubule, subsequently the loop of Henle, distal tubule and collecting duct

through which the filtrate reaches the bladder where it is excreted as urine. Compounds that are not filtered at the glomerulus move through peritubular capillaries which surround the proximal and distal tubules and *vasa recta* surrounding the loop of Henle and collecting ducts from where they may be absorbed into the tubular cells and from there into the tubular lumen via active and passive transport. Active and passive reabsorption from the tubular lumen may also occur back into tubular cells.

In the model developed here, compartments are defined which represent these key elements of the nephron (illustrated in Figure 2). Since tubular cells in the early proximal tubule (PT) section differ in morphology to those in later sections and the same holds for cells in collecting ducts (CD), these parts of the nephron are divided into three (PT1-3) and two (CD1-2) sections, respectively. The model used herein comprises eight blood compartments, representing arterial and venous blood vessels at different locations of the nephron (glomerular blood, proximal tubular blood sections 1-3, loop of Henle blood, distal tubular blood, collecting duct blood sections 1-2), and eight corresponding luminal compartments (i.e. glomerular space, proximal tubular lumen sections 1-3, loop of Henle lumen, distal tubular lumen, collecting duct lumen sections 1-2). Seven cellular compartments (proximal tubular cells sections 1-3, loop of Henle cells, distal tubular cells, collecting duct cells sections 1-2) connect to site-equivalent luminar and blood compartments via passive diffusion and active transport. Metabolism is incorporated in all cellular compartments. Figure 3 shows a schematic diagram of the mechanistic kidney model developed in this study including all compartments, flows and metabolism that are taken into account.

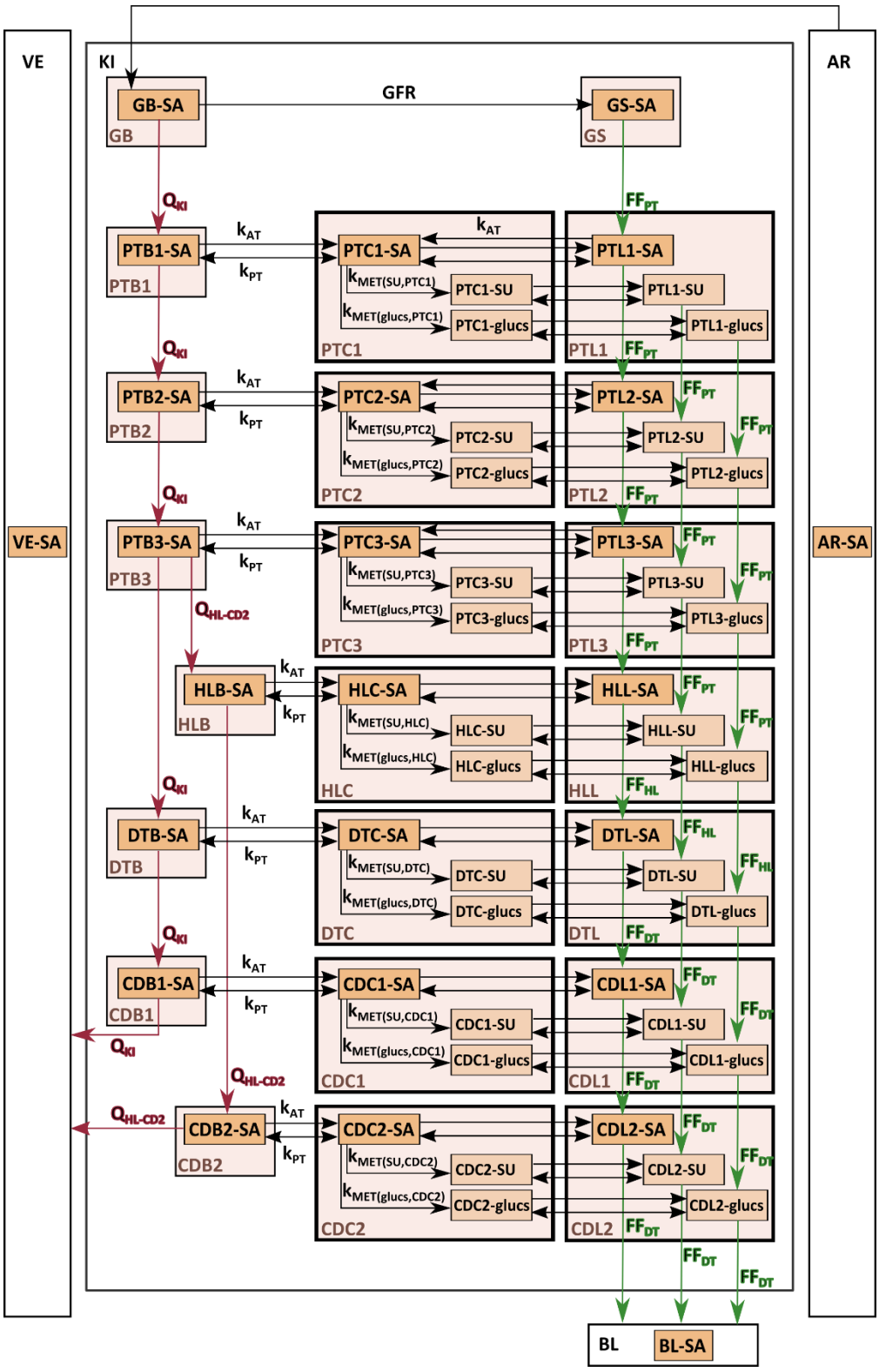


Figure 3: Schematic representation of the mechanistic kidney model. The central, white box labelled "KI" is the kidney compartment $(KI)$. The light orange boxes represent the compartments within the kidney model while the darker orange boxes represent concentrations of SA, SU and glucuronides. **Compartments**: GB = glomerular blood; GS = glomerular space;

PTB1-3 = proximal tubular blood 1-3; HLB = loop of Henle blood; DTB = distal tubular blood; CDB = collecting duct blood 1-2; PTC1-3 = proximal tubular cells 1-3; HLC = loop of Henle cells; DTC = distal tubular cells; CDC1-2 = collecting duct cells 1-2; PTL1-3 = proximal tubular lumen 1-3; HLL = Loop of Henle lumen; DTL = distal tubular lumen; CDL1-2 = collecting duct lumen 1-2; **Concentrations**: -SA = SA concentration in respective compartment; -SU = SU concentration in respective compartment; -glucs = glucuronide concentration in respective compartment; **Blood and fluid flows**: $GFR$ = glomerular filtration rate; $Q_{KI}$ = renal blood flow rate; $Q_{HL-CD2}$ = blood flow in loop of Henle and collecting ducts; $FF_{PT}$ = fluid flow leaving the glomerular space and proximal tubules; $FF_{HL}$ = fluid flow leaving the loop of Henle; $FF_{DT}$ = fluid flow leaving the distal tubules and collecting ducts; **Active transport**: single-sided arrows between blood and cellular, and between cellular and luminal concentrations with rate $k_{AT}$, equations presented in Appendix D.1 show that $k_{AT}$ represents added Michaelis-Menten terms of relevant active transport processes in the respective compartment; **Passive diffusion**: double-sided arrows between blood and cellular, and between cellular and luminal concentrations with rate $k_{PT}$; **Metabolism**: $k_{MET}$ = rate of metabolism to form SU or glucuronides in a subcompartment, Eq. 9-20 of Appendix D.1.2 show that $k_{MET}$ represents added Michaelis-Menten terms of relevant metabolic reactions in the respective compartment; exposure is entering the kidney compartment from the arterial blood compartment $(AR)$ and moves from the kidney compartment into the bladder $(BL)$ or the venous blood compartment $(VE)$.

The estimation of all compartment volumes is discussed in detail in Appendix A. Table 1 summarises all compartment volumes applied to the kidney model based on a young and healthy 70 kg individual.

Table 1: Compartment volumes of the kidney model representative of a young and healthy individual

| **Compartment volumes** | **Parameter value (mL)** | **References; derivation of parameter value** |
|---|---|---|
| Glomerular blood ($V_{GB}$) | 7.64 | Rouiller, 1969; scaling see Appendix A.1.4.1 |
| Proximal tubular blood 1 ($V_{PTB1}$) | 2.56 | 27.5 % of cortical peritubular blood |
| Proximal tubular blood 2 ($V_{PTB2}$) | 2.56 | 27.5 % of cortical peritubular blood |
| Proximal tubular blood 3 ($V_{PTB3}$) | 2.56 | 27.5 % of cortical peritubular blood |
| Loop of Henle blood ($V_{HLB}$) | 11.78 | 36.4 % of medullary blood |
| Distal tubular blood ($V_{DTB}$) | 1.63 | 17.5 % of cortical peritubular blood |
| Collecting duct blood 1 ($V_{CDB1}$) | 6.55 | 20.2 % of medullary blood |
| Collecting duct blood 2 ($V_{CDB2}$) | 14.07 | 43.4 % of medullary blood |
| | | |
| Proximal tubular cells 1 ($V_{PTC1}$) | 18.49 | See Appendix A (Eq. A.2; Table A.2; scaling in A.1.4.1) |
| Proximal tubular cells 2 ($V_{PTC2}$) | 18.49 | See Appendix A (Eq. A.2; Table A.2; scaling in A.1.4.1) |
| Proximal tubular cells 3 ($V_{PTC3}$) | 14.27 | See Appendix A (Eq. A.2; Table A.2; scaling in A.1.4.1) |
| Loop of Henle cells ($V_{HLC}$) | 26.80 | See Appendix A (Eq. A.3; Table A.2; scaling in A.1.4.2) |
| Distal tubular cells ($V_{DTC}$) | 8.30 | See Appendix A (Eq. A.2; Table A.2; scaling in A.1.4.1) |
| Collecting duct cells 1 ($V_{CDC1}$) | 22.60 | See Appendix A (Eq. 4.2; Table A.2; scaling in A.1.4.2) |
| Collecting duct cells 2 ($V_{CDC2}$) | 29.16 | See Appendix A (Eq. 4.2; Table A.2; scaling in A.1.4.2) |
| | | |
| Glomerular space ($V_{GS}$) | 3.57 | Rouiller, 1969; $V_{G\_total} - V_{GB}$; for a total glomerular volume ($V_{G\_total}$) averaging $44$ mm$^3$ per g kidney; scaling see Appendix A.1.4.1 |

| | | |
|---|---|---|
| Proximal tubular lumen 1 ($V_{PTL1}$) | 12.38 | See Appendix A (Eqs. A.2 and A.4; Table 4.2; scaling see A.1.4.1) |
| Proximal tubular lumen 2 ($V_{PTL2}$) | 12.38 | See Appendix A (Eqs. A.2 and A.4; Table 4.2; scaling see A.1.4.1) |
| Proximal tubular lumen 3 ($V_{PTL3}$) | 16.60 | See Appendix A (Eqs. A.2 and A.4; Table 4.2; scaling see A.1.4.1) |
| Loop of Henle lumen ($V_{HLL}$) | 14.20 | See Appendix A (Eqs. A.3 and A.5; Table 4.2; scaling see A.1.4.2) |
| Distal tubular lumen ($V_{DTL}$) | 11.35 | See Appendix A (Eqs. A.2 and A.4; Table 4.2; scaling see A.1.4.1) |
| Collecting duct lumen 1 ($V_{CDL1}$) | 3.51 | See Appendix A (Eqs. A.2 and A.4; Table 4.2; scaling see A.1.4.2) |
| Collecting duct lumen 2 ($V_{CDL2}$) | 18.57 | See Appendix A (Eqs. A.2 and A.4; Table 4.2; scaling see A.1.4.2) |
| | | |
| Bladder ($V_{BL}$) | 350 | Lukacz et al., 2011; average value |
| Arterial blood ($V_{AR}$) | 1698 | Peters, 2008a |
| Venous blood ($V_{VE}$) | 3396 | Peters, 2008a |

### 2.1.2 Blood flow, fluid flow and glomerular filtration rates

The change in concentration of a compound within each renal compartment over time is represented by ODEs that conserve mass balance. All ODEs for the mechanistic kidney model are compiled in Appendix D.1. The change in concentration within each compartment is driven by physiological flow rates and compound-specific parameters. Physiological flow rates such as the blood flow or fluid flow at different sections of the tubular lumen are presented in Table 2. A detailed discussion of these values is included in Appendix A (see A.2).

Table 2: Physiological flow rates at different sections of the tubular lumen

| **Flow rates** | **Parameter value (mL/min)** | **References** |
|---|---|---|
| Renal blood flow ($Q_{KI} = QC \times FQ_{KI}$) | 1100 | Bernareggi and Rowland, 1991; Peters, 2008a; Boroujerdi, 2015 |
| Blood flow in loop of Henle and collecting ducts 2 ($Q_{HL-CD2}$) | 100 | Eaton and Pooler, 2013 |
| Glomerular filtration rate ($GFR$) | 120 | Neuhoff et al., 2013; mL of water/min |
| Fluid flow leaving glomerular space and proximal tubules ($FF_{PT}$) | 45 | Neuhoff et al., 2013 |
| Fluid flow leaving loop of Henle ($FF_{HL}$) | 25 | Neuhoff et al., 2013 |
| Fluid flow leaving distal tubules and collecting ducts ($FF_{DT}$) | 12 | Neuhoff et al., 2013 |

$QC$ = cardiac output (6338 mL/min); $FQ_{KI}$ = fractional tissue blood flow in the kidney (0.174)

Compound-specific parameters relate to active and passive transport between the cellular, blood and luminal compartments, and metabolic activities. As mentioned earlier, this mechanistic model is developed to explore the kinetics of SA at the kidney level. The following section describes the kinetics of SA and all compound-specific parameters used in this model to simulate active and passive transport, as well as metabolic activity.

### 2.2 Prediction of SA-specific kinetics in the kidney: GFR, active and passive transport, and metabolic activity

The key kinetic processes of SA incorporated in the kidney model are glomerular filtration, active secretion and reabsorption, passive secretion and reabsorption, and metabolism. The key

metabolites of SA include salicyluric acid (SU) and acyl and phenolic glucuronides (glucs) all of which are considered in this kidney model.

### 2.2.1 Glomerular filtration rate of SA

SA reaches the kidney via the renal artery represented by the glomerular blood compartment. From there, compounds with a molecular weight of about 60,000 Dalton and lower are filtered into the glomerular space from where they flow into the proximal tubular lumen and later luminal compartments as part of the urinary filtrate (Boroujerdi, 2015). Clearance of substances from glomerular blood ($CL_{GB}$) by glomerular filtration is typically presented as the product of the glomerular filtration rate ($GFR$) and the fraction of the compound unbound in the plasma ($f_{u(p)}$) (Tucker, 1981; Rowland, 1984; Janků, 1993; Fenton and Praetorius, 2015) as shown in Eq. 1:

$$CL_{GB} = GFR\, f_{u(p)} \quad (1)$$

Please refer to Table 2 for the value of GFR. Approximately 20% of SA is free in plasma (therefore $f_{u(p)} = 0.2$), indicating approximately 80% of SA is bound to plasma proteins, such as albumin, and therefore is not readily filtered (Navar, 2009; Tojo and Kinugasa, 2012). The fraction not undergoing glomerular filtration passes into peritubular capillaries surrounding the proximal tubules. Through active transport and passive diffusion, SA may be secreted from the proximal tubular blood into proximal tubular cells, and from there into the proximal tubular lumen or reabsorbed from there back into the blood.

### 2.2.2 Active transport of SA in the kidney

Active transport is a saturable process and typically expressed as a Michaelis-Menten term (Felmlee et al., 2010, 2013; Ménochet et al., 2012a; Boroujerdi, 2015) as presented in Eq. 2:

$$k_{AT(T)} = \frac{J_{\max(T)}\, C_i}{K_{m(T)} + C_i} \qquad (2)$$

where $k_{AT(T)}$ is the rate of active transport via transporter protein $T$, $J_{\max(T)}$ is the maximum rate of transport or flux via transporter $T$, $K_{m(T)}$ is the Michaelis-Menten constant which represents the affinity of the transporter $T$ for its substrate and $C_i$ the concentration of SA in compartment $i$ in which a drug concentration increases or decreases due to active transport.

For SA, transporter inhibition and kinetics studies have been performed for OAT1, OAT2, OAT3, OAT4, MRP2, MRP4, BCRP, URAT1 and NPT1 (Sekine et al., 1998; Cha et al., 2000; Deguchi et al., 2002; Takeda et al., 2002; Khamdang et al., 2002; El-Sheikh et al., 2007; Matsson et al., 2007; Nozaki et al., 2007; Iharada et al., 2010; Ohtsu et al., 2010; Sedykh et al., 2013). However, data on active transport rates are scarce. A comprehensive discussion on the $K_m$ and $J_{max}$ values sourced from the literature and the scaling of $J_{max}$ values from the *in vitro* level to their equivalence of whole kidney mass for a young and healthy 70 kg individual is included in Appendix A.3. As discussed in more detail in Appendix A.3, additional scaling factors have been proposed, including relative activity factors (RAFs) which account for *in vitro-in vivo* differences in activity based on the transporter related intrinsic clearance ($CL_{int,t}$) or differences between animal and human activity (Neuhoff et al., 2013). RAFs are only considered for simulation results with initial parameters (see 3.2; results with and without RAFs are presented) and not taken into account for the sensitivity analysis and scans. Table 3 shows the transporter proteins which are taken into account in this model, i.e. OCT2, OAT1, OAT2, OAT3, OAT4, URAT1 and NPT1, their direction, $J_{\max}$ and $K_m$ values used, whether these are established for SA or another compound, in human or animal cells. Active transport with all these transporters is factored in in all proximal tubular compartments. Other models (Neuhoff et al., 2013; Huang and Isoherranen, 2018) only consider active transport in the proximal tubules. However, evidence exists indicating the

presence of active transport mechanisms in the renal medulla and collecting ducts (Madsen et al., 1988; Pearce et al., 2015). Also, when validating the performance of the model with excretion data reported by Levy (1965), initial simulations show that passive diffusion is insufficient to achieve the almost complete excretion of SA within 39 hours. Therefore, the OAT1 active transport term is included at each level of the nephron to reach the rate of excretion observed in healthy volunteers.

As plasma protein binding is found to affect active (as well as passive) drug transport in the Caco-2 cell model (Neuhoff et al., 2006), only the unbound fraction of drug concentration is considered to be relevant for active transport from blood to cellular compartments.

Table 3: Transporter proteins considered, their location and direction, and $J_{max}$ and $K_m$ values utilised in this model

| **Transporter ($T$)** | **$J_{\max(T)}$ (µmol/min)** | **$K_{m(T)}$ (µM)** | **Compound** | **Cells/ species** | **Direction** | **Reference** |
|---|---|---|---|---|---|---|
| OCT2 | 0.0432 | 28.7 | *Para*-amino-salicylic acid | HEK | PTB → PTC | Parvez et al., 2017 |
| OAT1 | 1.16 | 78 | *Para*-amino-salicylic acid | HEK | PTB → PTC | Parvez et al., 2017 |
| OAT2 | 15.3 [1] | 88.8 [2] | Creatinine[1]/ SA[2] | HEK[1]/ rat liver cells[2] | PTB → PTC | [1] Shen et al., 2015 / [2] Sekine et al., 1998 |
| OAT3 | 0.961 | 100 | *Para*-amino-salicylic acid | HEK | PTB → PTC | Parvez et al., 2017 |
| OAT4 | 22.4 | 172 | Perfluoro-octanoate | HEK | PTC → PTL<br>PTL → PTC | Yang et al., 2010 |
| NPT1 | 78.2 | $1.9 \times 10^3$ | SA | Mouse protein | PTC → PTL | Iharada et al., 2010 |
| URAT1 | 8.96 [1] | 25.3 [2] | Perfluoro-octanoate [1] / SA [2] | HEK | PTL → PTC | [1] Yang et al., 2010 / [2] Ohtsu et al., 2010 |

HEK = human embryonic kidney; PTB = proximal tubular blood; PTC = proximal tubular cells. Up to three significant figures reported.

### 2.2.3 Active transport of SA metabolites

As described above for SA, active secretion terms are added on all levels of the nephron and collecting ducts since including active secretion only at proximal tubular segments is insufficient to achieve a nearly complete excretion of SA within 39 hours. Similar to these observations on SA, initial simulations indicated that active secretion is necessary for SA metabolites to achieve excretion rates similar to those reported by Levy (1965).

Glucuronides are reported to interact with hOAT3 (Weiner et al., 1960; Lien, 1975; Wolff et al., 2007) and SA shows a high affinity to hOAT1 (Motojima et al., 2002). Since SU and SA glucuronides appear to share the same mechanism of active secretion as SA, an active secretion term is included for SA metabolites from PTC1-3 to PTL1-3, HLC to HLL, DTC to DTL, CDC1 to CDL1 and CDC2 to CDL2 with estimated $K_m$ and $J_{max}$ values similar to those of OAT transporters, i.e. $K_{m(OATmets)} = 0.07$ µmol/mL and $J_{\max(OATmets)} = 20$ µmol/min.

### 2.2.4 Passive diffusion of SA and metabolites in the kidney

Passive diffusion is a bidirectional, non-saturable process and of particular relevance to the reabsorption of substances from the tubular lumen rather than secretion from renal blood and tubular cells (Ménochet et al., 2012a; Felmlee et al., 2013; Ducharme, 2016). In this kidney model, passive diffusion is included between blood and cellular, and cellular and luminal compartments of all parts of the nephron and collecting ducts. Ménochet et al. (2012b) present a quantitative structure-activity relationship (QSAR) for the logarithm of the unbound passive diffusion clearance ($P_{diff,u}$) observed in human hepatocytes based on the logarithm of the distribution coefficient at pH 7.4 ($log\ D_{7.4}$) as shown in Eq. 3. In the absence of any additional kidney specific data, it is assumed that the unbound passive diffusion clearance in human hepatocytes and human renal cells is the same. The physiological pH of blood is maintained close

to 7.4 and intracellular pH is typically assumed at the same level. Both the pH of the urine and the $pK_a$ of a compound determine the degree of ionisation of the compound (Ducharme, 2016). Urine pH may range from 4.6 to 8.0 (Cook et al., 2007) and is set at 7.4 for initial simulations, meaning that a high proportion of SA in the urine is unionised. An unionised species is more lipid soluble and therefore permeates the phospholipid bilayer of tubular membranes more easily than ionised species which leads to a high degree of passive reabsorption from the urine. Passive diffusion at lower urinary pH is discussed in Appendix A.5.5. Eq. 3 is used to account for passive diffusion of SA between all blood and cellular, as well as cellular and luminal, compartments.

$$Log\ P_{diff,u} = 0.632 \times log\ D_{7.4} - 0.314 \qquad (3)$$

Log D values at pH 7.4 of SA and its metabolites, i.e. salicyluric acid, SA acyl glucuronide and SA phenolic glucuronide, were calculated in the ACD/Percepta 14.0.0 (Build 2726) software and are presented in Table 4. An average $P_{diff,u}$ value for all glucuronides ($P_{diff,u_{glucs}}$) is calculated with the average of log D values of SA acyl glucuronide and SA phenolic glucuronide. Since the resulting $P_{diff,u}$ is given in $\frac{\mu L}{min \times 10^6\ cells}$, scaling to the PTC cell population of $20 \times 10^6$ per g of kidney is needed for all substances. The scaled $P_{diff,u}$ values for SA, SU and glucuronides are 0.3297, 0.0313 and $2.03 \times 10^{-3}$ mL/min, respectively. Table 4 summarises all Log D and $P_{diff,u}$ values of SA, SU and SA glucuronides at pH 7.4.

Table 4: Log D and resulting $P_{diff,u}$ values of SA and its glucuronide and salicyluric acid metabolites at pH 7.4

| **Substance (S)** | **Log D at pH 7.4** | $\boldsymbol{P_{diff,u(S)}}$ **(mL/min)** |
|---|---|---|
| SA | -1.45 | 0.330 |
| Salicyluric acid (SU) | -3.07 | 0.0313 |
| SA acyl glucuronide | -4.36 | NA |
| SA phenolic glucuronide | -5.54 | NA |
| Glucuronide average (glucs) | -4.95 | $2.03 \times 10^{-3}$ |

The passive diffusion term, in which the SA and metabolite $P_{diff,u}$ values are applied, is defined in Eq. 4.

$$k_{PT} = P_{diff} C_i - P_{diff} C_j \qquad (4)$$

where $C_i$ and $C_j$ are concentrations subject to passive diffusion , e.g. $C_{PTB1}$ and $C_{PTC1}$, or $C_{PTC1}$ and $C_{PTL1}$. All $k_{PT}$ terms are included in detail in the ODEs presented in Appendix D.1.

### 2.2.5 Metabolism of SA in the kidney

Many phase I and phase II enzymes expressed in hepatocytes are also found in proximal tubular cells. However, levels in proximal tubular cells typically reach only 5-20 % of those in hepatocytes (Jakobsson and Cinti, 1973; Lash et al., 2008). This is also true for UGT enzymes, whereas UGT1A9, UGT2B7 and, to a lesser extent, UGT1A6 are found to be significantly expressed in the kidney (Knights and Miners, 2010; Margaillan et al., 2015). These enzymes are considered in Knights et al. (2016) who determined scaling factors for an *in vitro – in vivo* extrapolation (IVIVE). *In vitro* data were extrapolated to clearance values expected for UGT1A9, UGT2B7 and UGT1A6 glucuronidation *in vivo.* Similar to Knights et al. (2016), *in vitro* data of SA glucuronidation via UGT1A9, UGT2B7 and UGT1A6 were sourced in this study and scaled (see below and Appendix A.4) to an *in vivo* clearance for each enzymatic reaction. In the kidney, SA is metabolised to

salicyluric acid, salicyl acyl glucuronide and salicyl phenolic glucuronide (Levy, 1965; Needs and Brooks, 1985). Similar to the mathematical representation of active transport, the Michaelis-Menten equation, as defined in Eq. 5, is used to express a metabolic reaction (Felmlee et al., 2010; Boroujerdi, 2015; Cornish-Bowden, 2015):

$$k_{MET(M,i)} = \frac{V_{\max(M,i)}\, C_i}{K_{m(M)} + C_i} \tag{5}$$

where $k_{MET}$ is the rate of metabolism, $M$ represents the metabolite resulting from this reaction, $C_i$ stands for the concentration in the compartment in which metabolism takes place, $V_{\max(M,i)}$ is the maximum rate of metabolism for the formation of metabolite $M$ in compartment $i$, $K_{m(M)}$ for the Michaelis-Menten constant for the formation of metabolite $M$.

While some evidence shows that glucuronidation catalysing enzymes, UGT2B7 and UGT1A, are relatively evenly distributed across the tubular parts of the kidney (excluding the vasculature, glomeruli and the proximal straight tubule) (Gaganis et al., 2007), other sources report the contrary (Boroujerdi, 2015). Since SA-specific data on metabolism rates in compartments subsequent to the proximal tubules are lacking, an even distribution across all cellular compartments of the proximal and distal tubule, loop of Henle and collecting duct is assumed here.

Similar to the scaling of transporter related $J_{max}$ values, $V_{max}$ values given in µmol/mg protein/min are scaled to the whole kidney level. Details on $J_{max}$ scaling are included in Appendix A.4. Since the $V_{max}$ of $SU$ is based on clinical data, no scaling is necessary for this value. For all three metabolism reactions – conjugation with glycine to form salicyluric acid (SU) and conjugation with glucuronic acid catalysed by UGT1A6, UGT1A9 and UGT2B7 to form the salicyl

phenolic and salicyl acyl glucuronides (SAPG and SAAG) – applied $V_{max}$ and $K_m$ values are presented in Tables 5 and 6.

In order to place the results of the kidney model in the context of whole-body kinetics, the kidney model is incorporated into a PBK model parameterised for ASA and SA used to predict ASA and SA concentrations.

Table 5: $V_{max}$ and $K_m$ values sourced from the literature to account for SA conjugation with glycine to form SU in cellular compartments

| **Metabolite** | **Parameter designation $(M)$** | **$V_{max(M)}$ (µmol/min)** | **$K_{m(M)}$ (µM)** | **Reference** |
|---|---|---|---|---|
| SU | $SU$ | 6.3 [1,2] (a) | 103.5 [2] | [1] Levy and Tsuchiya, 1972; [2] Bochner et al., 1981 |

(a)average of $V_{max}$ cited from Levy and Tsuchiya (1972) and Bochner et al. (1981)

Table 6: $V_{max}$ and $K_m$ values applied to account for SA glucuronidation in cellular compartments

| **Metabolite (catalysing enzyme)** | **Parameter designation $(M)$** | $K_{m(M)}$ **(µM)** | $V_{max(M,PTC1)}$ **(µmol/min)** | $V_{max(M,PTC2)}$ **(µmol/min)** | $V_{max(M,PTC3)}$ **(µmol/min)** | $V_{max(M,HLC)}$ **(µmol/min)** | $V_{max(M,DTC)}$ **(µmol/min)** | $V_{max(M,CDC1)}$ **(µmol/min)** | $V_{max(M,CDC2)}$ **(µmol/min)** |
|---|---|---|---|---|---|---|---|---|---|
| SAPG (UGT1A6) | $PhenUGT1A6$ | 40.7 | $9.69 \times 10^{-4}$ | $9.69 \times 10^{-4}$ | $7.48 \times 10^{-4}$ | $1.40 \times 10^{-3}$ | $4.35 \times 10^{-4}$ | $1.18 \times 10^{-3}$ | $1.53 \times 10^{-3}$ |
| SAAG (UGT1A6) | $AcylUGT1A6$ | 78.0 | $9.18 \times 10^{-4}$ | $9.18 \times 10^{-4}$ | $7.08 \times 10^{-4}$ | $1.33 \times 10^{-3}$ | $4.12 \times 10^{-4}$ | $1.12 \times 10^{-3}$ | $1.45 \times 10^{-3}$ |
| SAPG (UGT1A9) | $PhenUGT1A9$ | 94.2 | 0.0762 | 0.0762 | 0.0588 | 0.1105 | 0.0342 | 0.0932 | 0.1202 |
| SAAG (UGT1A9) | $AcylUGT1A9$ | 334.3 | 0.0162 | 0.0162 | 0.0125 | 0.0235 | 0.0073 | 0.0198 | 0.0256 |
| SAPG (UGT2B7) | $PhenUGT2B7$ | 1242 | 0.0145 | 0.0145 | 0.0112 | 0.0210 | 0.0065 | 0.0177 | 0.0228 |
| SAAG (UGT2B7) | $AcylUGT2B7$ | 1640 | 0.0094 | 0.0094 | 0.0072 | 0.0136 | 0.0042 | 0.0115 | 0.0148 |

Reference for values presented in Table 6: Kuehl et al., 2006.

## 2.3 Mechanistic model coupled to a PBK model

Details of the PBK model and its parameterisation for ASA and SA are outlined in Appendix B. Furthermore, a sensitivity analysis and fitting for plasma concentrations of ASA and SA in the extended PBK model are included in Appendix B.1.2. All fitted parameter values and the mechanistic kidney model are subsequently incorporated in the PBK model. In order to validate the mechanistic kidney model coupled to a PBK model, the kinetics and excretion of ASA, SA and SA metabolites are simulated following an oral dose of ASA and compared to respective experimental data reported by Levy (1965). Full details of this are included in Appendix C.1. Model validation in this context means that model performance is verified for the tested conditions.

## 2.4 Application of the kidney model to predict renal tubular concentrations of drugs in four virtual individuals: young and healthy, elderly at risk of CKD, elderly with mild renal impairment (RI) and elderly with moderate renal impairment

The mechanistic kidney model described above is set up with parameter values representing a young and healthy individual. However, acute renal failure or other adverse effects observed in the kidney are typically observed in elderly individuals or persons who have been diagnosed with a compromised renal function (Zhang et al., 2005). In order to establish to what degree renal tubular concentrations predicted for a young and healthy adult differ from those predicted for the elderly, three virtual elderly individuals are defined. For this, key parameters for which values are known to be decreased in the elderly at risk of CKD, as well as individuals with mild and moderate RI, are set accordingly.

2.4.1 Setting parameter values characterising: an elderly person at risk of CKD, an elderly person with mild renal impairment and an elderly person with moderate renal impairment

Key parameters are the GFR, cardiac output, cortical renal blood flow, rates determining the flow of urinary filtrate in the tubular lumen and the number of nephrons. In comparison to a young and healthy individual, the number of nephrons in an elderly person is roughly halved (Denic et al., 2017). Therefore, the tubular cell numbers used to scale transporter $J_{max}$ and $P_{diff,u}$ values are halved. In addition, the metabolism-related parameter $MPPGK$ is halved to scale SU and glucuronide $V_{max}$ values accordingly. All elderly-based $J_{max}$, $P_{diff,u}$ and $V_{max}$ values are presented in Appendix A.5. Also, urinary pH is decreased in two individuals, since at a low urine pH, a higher proportion of unionised substances (for acidic species) will be present which are readily reabsorbed via passive diffusion. Table 7 summarises physiological parameters amended in the three elderly individuals. Further details on all amended physiological parameters are included in Appendix A.5.

Table 7: Physiological parameters determining four cases, a young and healthy adult, an elderly person at risk of CKD, an elderly person with mild RI and an elderly person with moderate RI

| **Parameter** | **Young and healthy adult** | **Elderly, at risk of CKD** | **Elderly with mild RI** | **Elderly with moderate RI** |
|---|---|---|---|---|
| $GFR$ (mL/min) | 120 | 60 | 50 | 30 |
| $QC$ (mL/min) | 6,338 | 2,970 | 2,970 | 2,970 |
| $Q_{KI}$ (mL/min) | 1100 | 517 | 517 | 517 |
| $FF_{PT}$, $FF_{HL}$, $FF_{DT}$ (mL/min) | 45, 25, 12 | 45, 25, 12 | 30, 18, 8 | 30, 18, 8 |
| Urinary pH | 7.4 | 7.4 | 5.3 | 5.3 |
| Number of nephrons | $1 \times 10^6$ | $5 \times 10^5$ | $5 \times 10^5$ | $5 \times 10^5$ |

### 2.4.2 Dosing scenarios considered for all four individuals

For each of the four individuals – a young and healthy adult, an elderly person at risk of CKD, an elderly person with mild renal impairment and an elderly person with moderate renal impairment – three different scenarios are set which differ in the dose applied daily and the length of exposure. In the first scenario, a common low dose of 420 µmol/day (75 mg/day) (Petersen et al., 1989; The Salt Collaborative Group, 1991; Hansson et al., 1998; Derry, 2000; NHS, 2018; Mayo Clinic, 2019; MedicineNet, 2019) is applied relevant to doses used to prevent cardiovascular events. In the second scenario, a venous blood concentration of 2.2 µmol/mL is used as an initial concentration, since at therapeutic doses, a SA steady state concentration of up to 2.2 µmol/mL is reached (Furst et al., 1979; Needs and Brooks, 1985). The first two scenarios are simulated for a period of two weeks representing chronic exposure. Even though an exposure duration of two weeks with a dose applied once per day would be classified as sub-acute rather than chronic, the maximum concentration ($C_{max}$) reached in the proximal tubular cells on the first day is equal to the $C_{max}$ values reached on subsequent days. Also, under constant exposure, the steady state in the proximal tubular cells is reached after approximately 15-50 minutes (depending on the dose and virtual individual selected). Therefore, a two-week simulation period is judged to be adequate to represent chronic exposure. The third scenario represents a case of intoxication which requires therapeutic intervention at a salicylate plasma (in the model as venous blood) concentration of 3.24 µmol/mL (450 mg/L, mean of 400-500 mg/L as reported by Wood et al., 2005). The simulation period for this case is one day. All scenario data are shown in Table 8.

Table 8: Exposure levels, duration and simulation times used in three different exposure scenarios

| **Scenario** | **Dose (compartment, in which substance is applied)** | **Exposure time** | **Simulation time (min)** |
|---|---|---|---|
| Low therapeutic dose, chronic | 420 µmol (ASA, stomach undissolved) | Once a day | 20'160 (14 days) |
| High therapeutic dose, chronic | 2.2 µmol/mL (SA, venous blood) | Constant | 20'160 (14 days) |
| Intoxication, acute | 3.24 µmol/mL (SA, venous blood) | Constant | 1'440 (1 day) |

### 2.4.3 Local sensitivity analyses and scans for simulations with all four individuals

Local sensitivity analyses are performed on the impact of parameters used in the mechanistic kidney model, including $GFR$, $f_{u(p)}$, blood and filtrate flow rates ($QC$, $FQ_{KI}$, $Q_{HL-CD2}$, $FF_{PT}$, $FF_{HL}$, $FF_{DT}$), passive diffusion parameters ($P_{diff,u(SA)}$, $P_{diff,u(SU)}$, $P_{diff,u(glucs)}$), active transporter parameters ($J_{\max}$ and $K_{\mathrm{m}}$ values for $OAT_{mets}$ and the transporters OCT2, OAT1-4, NPT1 and URAT1) and metabolism parameters ($V_{\max}$ and $K_{\mathrm{m}}$ values for the formation of SU and salicyl phenolic and salicyl acyl glucuronides catalysed by UGT1A6, UGT1A9 and UGT2B7). The aim of the local sensitivity analysis is to identify parameters which, when perturbed (i.e. changed to a minor degree), have a high impact on the predicted SA and SU concentrations in PTC compartments. This is relevant since a certain degree of uncertainty underlies each of these parameters. Also, there will be inter-individual differences in blood flows, transporter expression or the rate of metabolism. Besides SA, concentrations for SU are taken into account, since about 70 to 80% of an oral dose of ASA is excreted in the form of SU (Levy, 1965; and Appendix C.1). The method underlying the local sensitivity analysis approach used here is explained in detail in Martins et al. (2000, 2001) and Ingalls and Sauro (2003).

Since it is important to understand how the behaviour of a model changes with a wide range of parameter values, the parameters which are identified in the local sensitivity analysis will subsequently be changed over a wider, biologically plausible range in scans (also termed global sensitivity analysis). As a result of this, a range of PTC concentrations is predicted which may reflect exposure levels in a variety of individuals for the dosing scenarios defined.

Predictions with initial parameters and scans are interpreted in relation to a hypothesised toxicity threshold of 90 µM in PTC compartments. This threshold is defined following the review of relevant toxicity data outlined in Appendix C.2.

## 3. Results

This study presents the development and validation of a new PBK coupled mechanistic kidney model which is used to investigate the quantitative relationship between therapeutic doses of SA and toxicity expected in proximal tubular cells of young and elderly virtual individuals. Proximal tubular cell (PTC1-3) concentrations are predicted for four virtual individuals and three exposure scenarios each totalling 12 simulation scenarios. Key results presented in Section 3.1 include the results of local sensitivity analyses which inform the choice of parameters for the performance of scans (global sensitivity analyses). Scan results help to interpret predictions with initial parameter values in the light of uncertainties surrounding parameters which have a high impact on predicted PTC concentrations. Scans and predictions with initial parameter values are included in Section 3.2 and presented in relation to the hypothesised toxicity threshold of 90 µM at which mitochondrial toxicity is expected in PTC compartments (as detailed in Appendix C.2).

### 3.1 Local sensitivity analysis results

#### 3.1.1 Chronic, low therapeutic dose of ASA

For all four individuals, both parameters determining the formation of SU, $V_{\max(SU)}$ and $K_{\mathrm{m}(SU)}$, are predicted to have moderate impact on the concentration of SA in the PTC1 compartment, high impact in PTC2 and highest impact in PCT3. The concentration of SU in all PTC compartments is highly influenced by parameters defining the rate of active transport of all metabolites, $J_{\max(OATmets)}$ and $K_{\mathrm{m}(OATmets)}$, in all four individuals. In the young, all PTC concentrations of SA and SU are moderately sensitive to the fraction unbound of SA ($f_{u(p)}$). In all three elderly individuals, $f_{u(p)}$ has a fairly low impact on all PTC concentrations. For the young and healthy adult and the elderly person at risk of CKD, the sensitivity analysis results for this dose are illustrated in Appendix C.3 (Figures C.1 and C.2).

#### 3.1.2 Chronic upper therapeutic dose reaching a SA venous blood concentration of 2.2 mM

At a constant SA venous blood concentration of 2.2 mM, SA concentrations in all PTC compartments are moderately influenced by parameters determining the rate of the active transport of SA via NPT1, $J_{\max(NPT1)}$ and to a lesser extent $K_{\mathrm{m}(NPT1)}$, in the young and the elderly at risk of CKD. In the elderly with mild RI, $f_{u(p)}$ has a high impact on SA concentrations in all PTC compartments, while $GFR$ and the urinary filtrate flow rate in the proximal tubular lumen ($FF_{PT}$) have a high impact in PTC1 and a lower impact on PTC2 and PTC3 concentrations. The elderly with moderate RI shows similar results to the elderly with mild RI, plus $J_{max(NPT1)}$ highly influences PTC1 concentrations as well as PTC2 and PTC3 concentrations to a lesser extent. Sensitivity analysis results are shown in Figure 4 and Appendix C.3 (Figure C.3) for the elderly individuals with mild and moderate RI, respectively. SU concentrations are highly sensitive to the $V_{max}$ of SU formation ($V_{\max(SU)}$) and to the active transport of metabolites ($J_{\max(OATmets)}$ and to a lower extent $K_{\mathrm{m}(OATmets)}$) in the young, the elderly at risk of CKD and the elderly with

mild RI. In the elderly with moderate RI, all parameters appear to have a minor impact on SU concentrations.

### 3.1.3 Acute intoxication at 3.24 mM SA venous blood concentration

Results of sensitivity analyses related to a constant SA venous blood concentration of 3.24 mM for 24 hours are equal or very similar to the results outlined above for a 14-day constant SA venous blood concentration of 2.2 mM for the young, the elderly at risk of CKD and the elderly with mild RI. At this exposure, $J_{max(NPT1)}$ has less impact on PTC SA concentrations in the elderly with moderate RI. So, the parameters mainly influencing SA concentrations are the same as those reported for the elderly with mild RI. Results are specifically shown in Appendix C.3 (Figure C.4) for the elderly person with moderate RI.

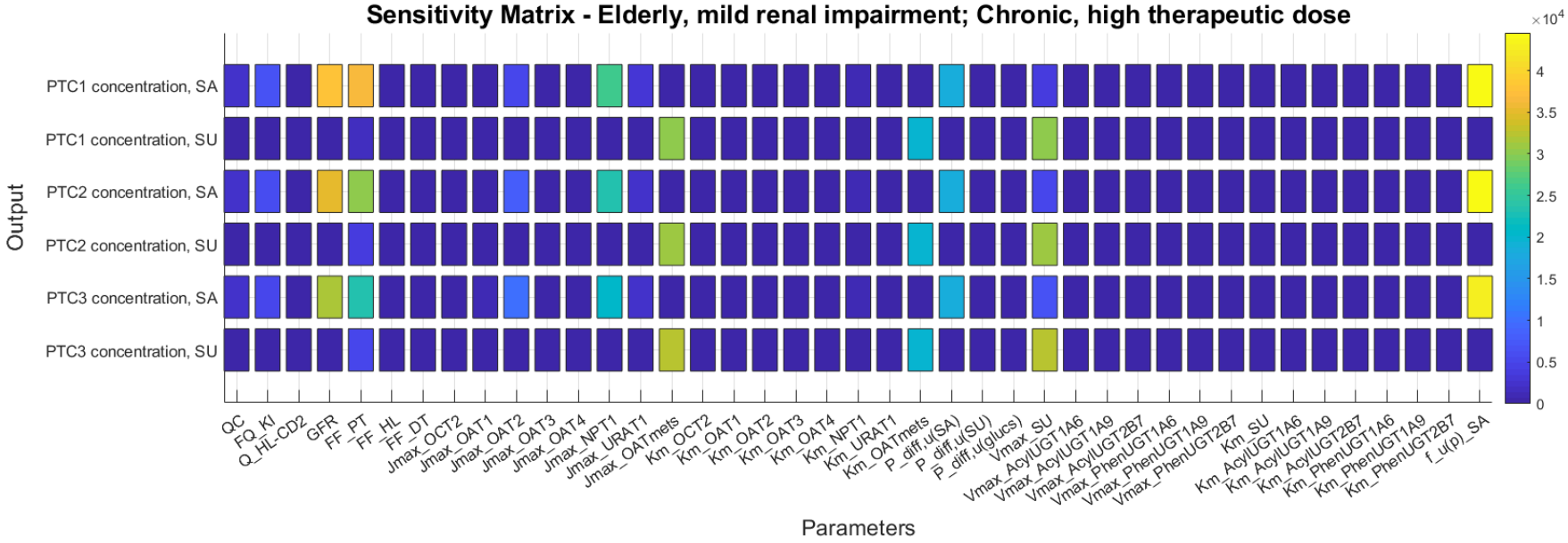


Figure 4: Time-integral sensitivity coefficients ($S_q$), giving an indication of the total sensitivity of the model parameters as indicated on the x-axis on the predicted PTC concentrations of SA and SU following the oral administration of a chronic, high therapeutic dose of ASA in the elderly with mild RI. A high value (colour-coded in yellow) indicates a high sensitivity and, therefore, small changes in this model parameter would cause large changes to PTC concentrations of SA and SU. Lower values are colour-coded in blue.

All parameters that have been identified to have the most impact on predicted proximal tubular concentrations are presented in Table 11 and included in scans over a predefined range in Section 3.2.

## 3.2 Results of predictions with initial parameter values and scans over predefined ranges

Here, we first present simulation results with initial parameters with and without the consideration of RAFs. The application of RAFs to scale transporter terms of OCT2, OAT1, OAT2 and OAT3 is explained in Appendix A.3. For each of the parameters identified in local sensitivity analyses, biologically plausible ranges are defined in Section 3.2.2. These ranges determine the span over which parameter values change over five steps using the scans function in SimBiology. Scan results and more details on predictions with initial parameter values (without RAFs) are then presented in relation to the hypothesised toxicity threshold for SA of 90 µM in PTC compartments (as detailed in Appendix C.2).

### 3.2.1 Results of predictions with initial parameters: with and without RAFs

Tables 9 and 10 show the highest predicted $C_{max}$ for SA across PTC1-3 compartments when the model is simulated with the parameter values sourced from the literature without and with the application of RAFs, respectively. Generally, for any of the scenarios, the $C_{max}$ in PTC1 is very similar to the $C_{max}$ in PTC2 and PTC3. Therefore, only the highest $C_{max}$ across all PTC compartments are presented in Tables 9 and 10. For initial parameter simulations without RAFs, all $C_{max}$ values are detailed in 3.2.3-3.2.5.

Table 9: SA $C_{max}$ concentrations (in mM) predicted with initial parameters for the four individual cases exposed at three different dose levels (without RAFs)

| | **Maximum PTC concentration at chronic, low therapeutic dose (mM) (compartment)** | **Maximum PTC concentration at chronic, high therapeutic dose (mM) (compartment)** | **Maximum PTC concentration at acute intoxication (mM) (compartment)** |
|---|---|---|---|
| **Young and healthy adult** | 0.0044 (PTC1) | 0.484 (PTC3) | 0.520 (PTC3) |
| **Elderly, at risk of CKD** | 0.0100 (PTC1) | 0.587 (PTC3) | 0.628 (PTC2) |
| **Elderly with mild RI** | 0.0110 (PTC1) | 63.9 (PTC1) | 127 (PTC1) |
| **Elderly with moderate RI** | 0.0098 (PTC1) | 18.1 (PTC1) | 52.8 (PTC1) |

Table 10: SA $C_{max}$ concentrations (in mM) predicted with initial parameters for the four individual cases exposed at three different dose levels (with RAFs)

| | **Maximum PTC concentration at chronic, low therapeutic dose (mM) (compartment)** | **Maximum PTC concentration at chronic, high therapeutic dose (mM) (compartment)** | **Maximum PTC concentration at acute intoxication (mM) (compartment)** |
|---|---|---|---|
| **Young and healthy adult** | 0.0118 (PTC1) | 3.00 (PTC3) | 3.22 (PTC3) |
| **Elderly, at risk of CKD** | 0.0253 (PTC1) | 12.2 (PTC2) | 13.6 (PTC3) |
| **Elderly with mild RI** | 0.0294 (PTC1) | 189 (PTC3) | 246 (PTC1) |
| **Elderly with moderate RI** | 0.0288 (PTC1) | 161 (PTC3) | 186 (PTC3) |

### 3.2.2 Application of local sensitivity analysis results for scans: Definition of parameter ranges

As mentioned earlier, the parameter values highlighted in the sensitivity analyses performed for each of the 12 simulation scenarios (4 individuals and 3 dosing conditions) change over five steps spread over a predefined range. All parameter values selected for each scenario are presented in Table 11 and ranges designated for these parameters are shown in Table 12. Scans were performed over the same simulation times as those applied for sensitivity analyses (as defined in Section 2.4.2). When performing the scans for more than two parameters simultaneously over 20'160 minutes, an error occurs in SimBiology. Therefore, for scans with four parameters, scan performance times are amended to 10'080 minutes.

Table 11: Parameters identified to have the most impact on SA concentrations in PTC compartments for the simulation scenarios tested

| | **Chronic, low therapeutic dose** | **Chronic, high therapeutic dose** | **Acute intoxication** |
|---|---|---|---|
| **Young and healthy adult** | $V_{\max(SU)}$, $K_{\mathrm{m}(SU)}$ | $J_{\max(NPT1)}$ | $J_{\max(NPT1)}$ |
| **Elderly, at risk of CKD** | $V_{\max(SU)}$, $K_{\mathrm{m}(SU)}$ | $J_{\max(NPT1)}$ | $J_{\max(NPT1)}$ |
| **Elderly with mild RI** | $V_{\max(SU)}$, $K_{\mathrm{m}(SU)}$ | $f_{u(p)_{SA}}, GFR$ | $f_{u(p)_{SA}}, GFR$ |
| **Elderly with moderate RI** | $V_{\max(SU)}$, $K_{\mathrm{m}(SU)}$ | $f_{u(p)_{SA}}, GFR, FF_{PT}$ $J_{\max(NPT1)}$ | $f_{u(p)_{SA}}, GFR$ |

Table 12: Ranges over which parameter values will be changed using the scans function in SimBiology

| **Parameter** | **Initial value, young and healthy adult** | **Initial value, elderly individuals** | **Range** |
|---|---|---|---|
| $f_{u(p)_{SA}}$ (dimensionless) | 0.40 | 0.65 | 0.07 – 0.75 |
| $V_{\max(SU)}$ (µmol/min) | 6.3 | 3.15 | 1.6 – 12.6 |
| $K_{\mathrm{m}(SU)}$ (mM) | 0.104 | 0.104 | 0.0109 – 0.197 |
| $J_{\max(NPT1)}$ (µmol/min) | 78.2 | 39.1 | 0.0432 – 782 |
| $GFR$ (mL/min) | 120 | 30-60 | 5 – 150 |
| $FF_{PT}$ (mL/min) | 45 | 30 | 20 – 60 |

The fraction unbound of salicylic acid is fitted to 0.65 for the virtual elderly which is on the higher end of the wide spectrum of unbound fractions reported for SA, as indicated in Appendix B.1.2.3, and considered adequate for toxic SA blood concentrations. The lower bound of reported $f_{u(p)}$ values lies at approximately 0.07 (Furst et al., 1979) and an upper bound is set at 0.75. For the rate of SU formation, the widest range (mean ± standard deviation) of $V_{max}$ and $K_m$ values is found in Roberts et al. (1983) who included values for both young adults and elderly individuals. The maximum $K_m$ and $V_{max}$ values are based on the young group and the minimum $K_m$ is based on the elderly group. The minimum $V_{max}$ of both groups is 3.8 µmol/min and therefore slightly higher than the $V_{\max(SU)}$ for the three elderly cases set at 3.15 µmol/min. In order to account for uncertainty underlying the measured value, the lower bound of the $V_{\max(SU)}$ range is set at 1.6 µmol/min. The $J_{\max(NPT1)}$ value taken from the literature is established with mouse protein and judged to exhibit similar transporter kinetics in human cells. Since the $J_{\max}$of NPT1 is the highest $J_{\max}$ value used in this model, the higher bound is selected an order of magnitude higher than the literature value. The lower bound is set at 0.0432 µmol/min which is the lowest $J_{\max}$value used in this model (for OCT2). The $GFR$ observed with normal kidney function may reach up to approximately 140 mL/min/1.73 $m^2$ body surface area of an adult (Weinstein and

Anderson, 2010; Delanaye et al., 2012), whereas a value below 15 mL/min is associated with kidney failure (USRDS, 2017). For the scans, a $GFR$ range is set with a minimum of 5 mL/min and a maximum of 150 mL/min. The rate at which urinary filtrate flow through the proximal tubular lumen is set at 45 mL/min for the young (Neuhoff et al., 2013) and estimated at 30 mL/min for the elderly individuals. In order to account for uncertainty underlying both values, the $FF_{PT}$ range is defined from 20 to 60 mL/min.

### 3.2.3 Detailed simulation and scan results: chronic, low therapeutic dose of ASA

When the model is simulated with the initial $V_{\max(SU)}$ and $K_{\mathrm{m}(SU)}$ values for the young and healthy adult, PTC1, PTC2 and PTC3 concentrations plateau at 0.0044, 0.0034 and 0.0029 mM, respectively. In the elderly at risk of CKD and initial $V_{\max(SU)}$ and $K_{\mathrm{m}(SU)}$ values, maximum PTC1, PTC2 and PTC3 concentrations are predicted at 0.0100, 0.0087 and 0.0071, respectively. These are very similar to concentrations predicted for the elderly with moderate RI, i.e. 0.0098, 0.0088 and 0.0072 mM, respectively. For the elderly with mild RI, maximum PTC1, PTC2 and PTC3 concentrations are predicted at 0.0110, 0.0090 and 0.0070 mM, respectively, when simulated with initial $V_{\max(SU)}$ and $K_{\mathrm{m}(SU)}$ values. With any of the values included in the scan, no maximum concentration in PTC1-3 compartments exceeds 0.03 mM for all four virtual individuals. Figure 5 shows $C_{max}$ values predicted for the elderly individual with mild RI in each PTC compartment over the scan ranges of $V_{\max(SU)}$ values.

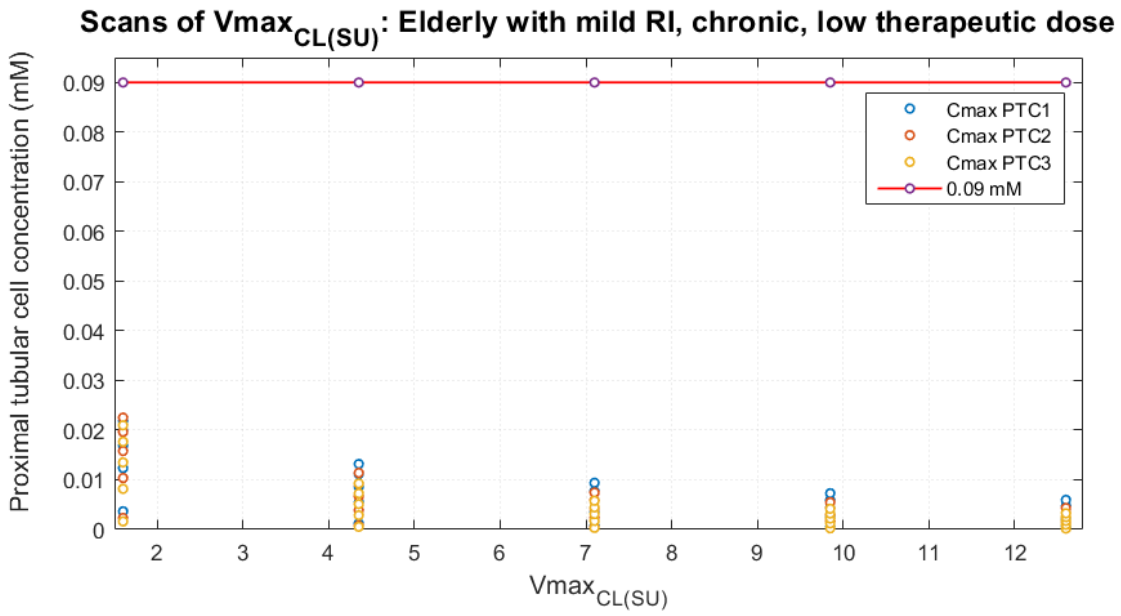


Figure 5: $C_{max}$ values predicted for the elderly individual with mild RI in each PTC compartment over the scan ranges of $V_{\max(SU)}$ values, in relation to the defined threshold of toxicity at 0.09 mM (scans with $V_{\max(SU)}$ and $K_{m(SU)}$ simultaneously).

### 3.2.4 Detailed simulation and scan results: chronic, upper therapeutic dose reaching a SA venous blood concentration of 2.2 mM

For the young and healthy adult, PTC1, PTC2 and PTC3 concentrations plateau at 0.481, 0.481 and 0.484 mM, respectively, when the model is run with the initial $J_{\max(NPT1)}$ at 78.2 µmol/min. A scan including five steps over the range of 0.0432 to 782 µmol/min for $J_{\max(NPT1)}$ shows that for a value close to 600 µmol/min, PTC1-3 concentrations reach their maxima at around 0.09 mM. At lower $J_{\max(NPT1)}$ values PTC concentrations plateau at a level exceeding the 0.09 mM threshold, and at higher $J_{\max(NPT1)}$ values maximum PTC concentrations are below it. For the elderly individual at risk of CKD, maximum concentrations in PTC1, PTC2 and PTC3 with the initial

$J_{\max(NPT1)}$ are at 0.584, 0.586 and 0.587 mM, respectively. When simulated with initial parameter values for the elderly with mild RI, PTC1, PTC2 and PTC3 concentrations reach 63.9, 51.4 and 42.3 mM, respectively. For the elderly with moderate RI, lower PTC concentrations are calculated, namely between 18.1 and 16.7 mM, likely due to the lower GFR and resulting lower PTL concentrations of which lower levels are reabsorbed into PTC compartments.

The scan for the elderly individual at risk of CKD indicates that at a $J_{\max(NPT1)}$ of 391 µmol/min and higher, maximum PTC1-3 concentrations are below 0.09 mM while at 196 µmol/min and lower, PTC1-3 concentrations plateau at a level above the threshold. Figure 6 shows $C_{max}$ values predicted for the elderly individual at risk of CKD in each PTC compartment over the scan ranges of $J_{\max(NPT1)}$.

For the elderly with moderate RI, scans with $f_{u(p)SA}$, $GFR$, $FF_{PT}$ and $J_{max(NPT1)}$ simultaneously generate predicted $C_{max}$ values over a wide range at each step of each parameter (>3 orders of magnitude) (results not shown). This is expected as the defined ranges, in particular for $J_{\max(NPT1)}$, are fairly wide. Therefore, scans for this scenario are split. Scans performed with $f_{u(p)SA}$ and $GFR$ simultaneously, and $FF_{PT}$ and $J_{max(NPT1)}$ simultaneously show that $FF_{PT}$ clearly has the least impact on predict $C_{max}$ values and that nearly all predicted $C_{max}$ value are above the toxicity threshold of 0.09 mM. Figures 7 and 8 shows results for the elderly with moderate RI over the scan ranges of $J_{\max(NPT1)}$ and $f_{u(p)SA}$, respectively.

For the elderly with mild RI, scans for $f_{u(p)SA}$ and $GFR$ are very similar to those obtained for the elderly with moderate RI.

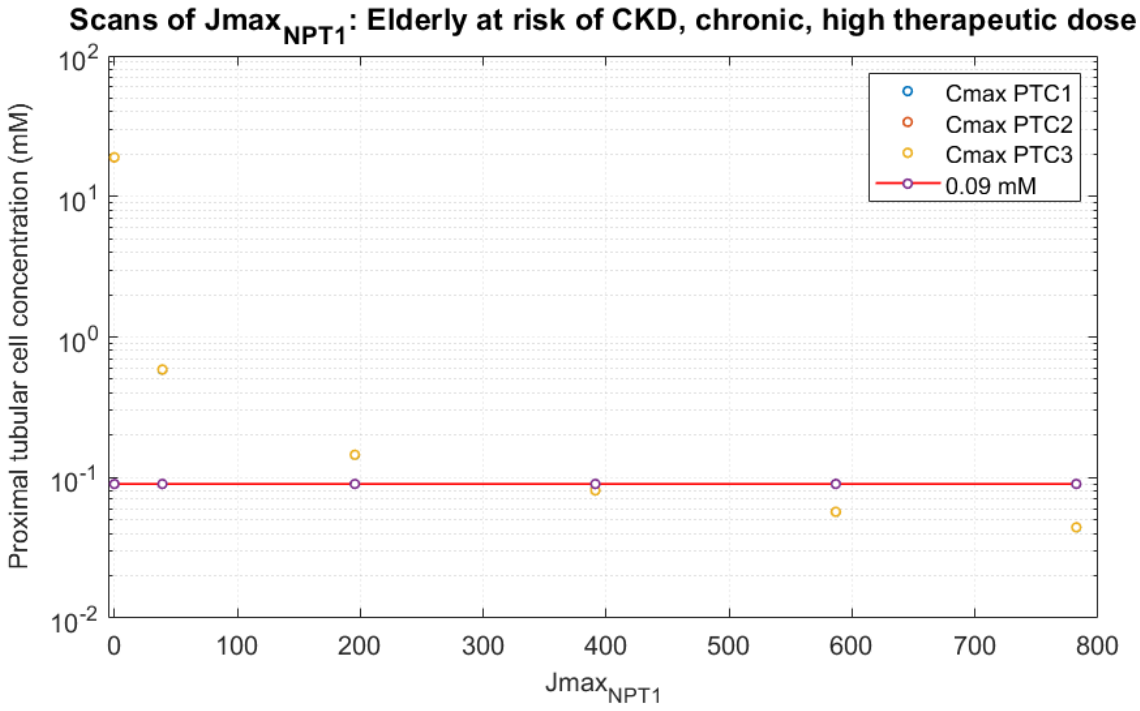


Figure 6: $C_{max}$ values predicted for the elderly individual at risk of CKD in each PTC compartment over the scan ranges of $J_{\max(NPT1)}$, in relation to the defined threshold of toxicity at 0.09 mM. Predicted $C_{max}$ values for PTC3 are superimposed on the predicted $C_{max}$ values for PTC1 and PTC2.

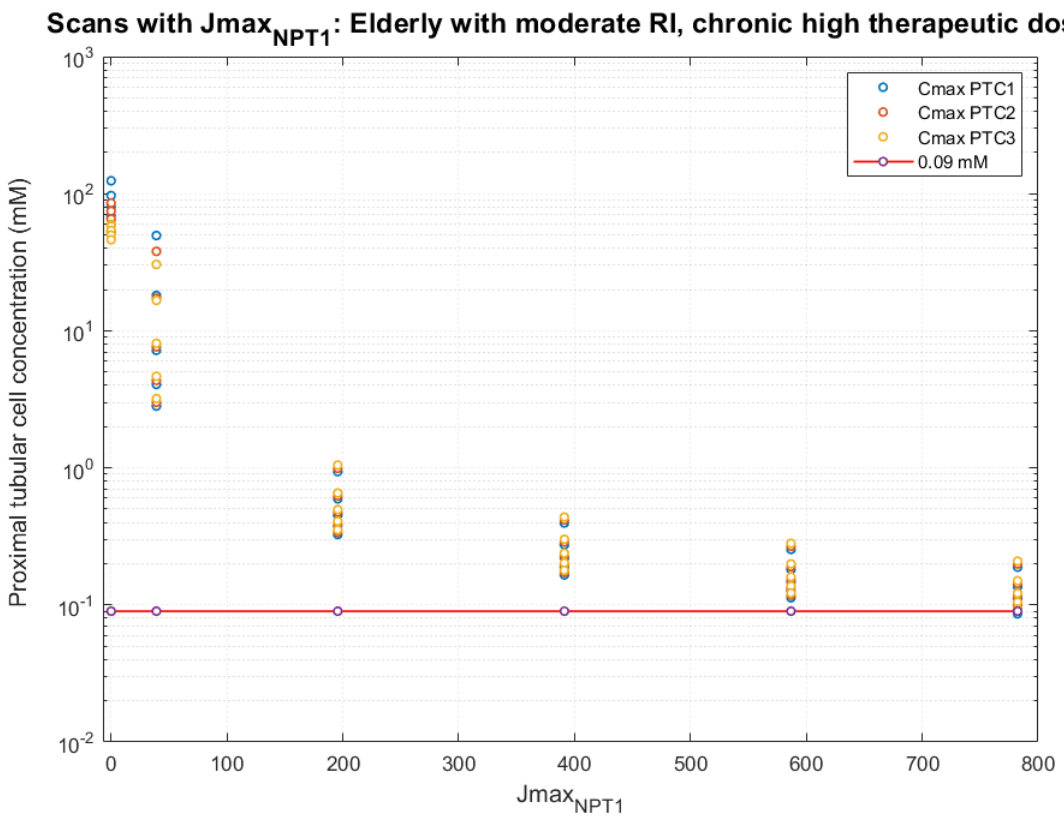


Figure 7: $C_{max}$ values predicted for the elderly individual with moderate RI in each PTC compartment over the scan ranges of $J_{\max(NPT1)}$, in relation to the defined threshold of toxicity at 0.09 mM (scans with $J_{\max(NPT1)}$ and $FF_{PT}$ simultaneously).

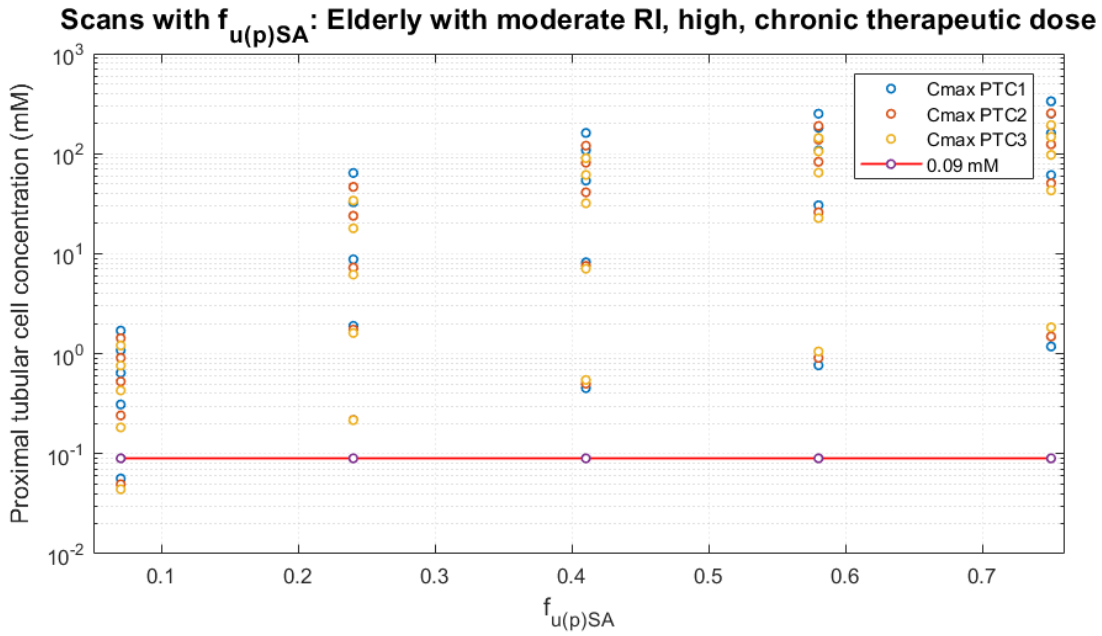


Figure 8: $C_{max}$ values predicted for the elderly individual with moderate RI in each PTC compartment over the scan ranges of $f_{u(p)SA}$, in relation to the defined threshold of toxicity at 0.09 mM (scans with $f_{u(p)SA}$ and $GFR$ simultaneously).

### 3.2.5 Detailed simulation and scan results: acute intoxication at 3.24 mM SA venous blood concentration

When the model is simulated with the initial $J_{\max(NPT1)}$, PTC1, PTC2 and PTC3 concentrations of the young and healthy adult are 0.517, 0.518 and 0.520 mM. A scan including five steps over the range of 0.0432 to 782.32 µmol/min for $J_{\max(NPT1)}$ shows slightly higher but very similar results as generated with the chronic upper therapeutic dose. At a SA venous blood concentration at 3.24 mM and a $J_{\max(NPT1)}$ value at 587 µmol/min, PTC1, PTC2 and PTC3 concentrations reach their maxima at 0.0965, 0.0967 and 0.0968 mM, respectively. Only the highest $J_{\max(NPT1)}$ value generates PTC values below 0.09 mM. For the elderly individual at risk of CKD, maximum concentrations in PTC1, PTC2 and PTC3 with the initial $J_{\max(NPT1)}$ are between 0.627and 0.628

mM, respectively. Scan results for the elderly at risk of CKD are also very similar to scan results generated with the chronic upper therapeutic dose for this individual.

When the model is simulated with initial $f_{u(p)_{SA}}$ and $GFR$ values for the elderly individual with mild RI, maximum concentrations in PTC1, PTC2 and PTC3 are at 127, 98.4 and 77.3 mM, respectively. Again, in comparison, lower but clearly toxic PTC concentrations are calculated for the elderly with moderate RI with the initial parameter values, i.e. 52.8, 43.6 and 36.9 mM for PTC1, PTC2 and PTC3, respectively. The $f_{u(p)_{SA}}$ and $GFR$ scan results for the elderly individual with mild RI at a SA venous blood concentration of 3.24 mM are similar to those obtained for the elderly with moderate RI. Figure 9 shows $C_{max}$ values predicted for the elderly individual with mild RI in each PTC compartment over the scan ranges of $GFR$. As expected, nearly all data points are above the 0.09 mM toxicity threshold.

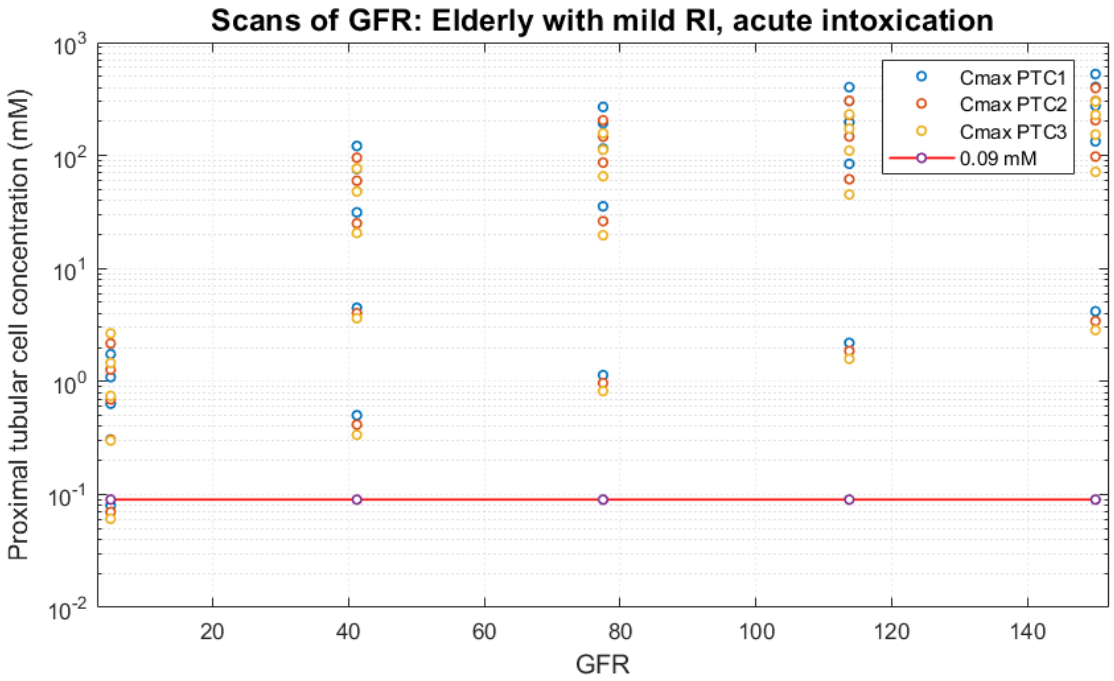


Figure 8: $C_{max}$ values predicted for the elderly individual with mild RI in each PTC compartment over the scan ranges of $GFR$, in relation to the defined threshold of toxicity at 0.09 mM (scans with $GFR$ and $f_{u(p)SA}$ simultaneously).

### 3.3 Key results

To sum up the results of the sensitivity analyses, values for the $V_{\max(SU)}$ and $K_{\mathrm{m}(SU)}$ significantly influence PTC concentrations at the chronic, low therapeutic dose, and $J_{\max(NPT1)}$, $f_{u(p)SA}$ and $GFR$ have the most impact on PTC concentrations at the two higher exposure scenarios. $V_{\max(SU)}$, $K_{\mathrm{m}(SU)}$ and $J_{\max(NPT1)}$ are parameters which contribute to the decrease of SA in PTC compartments – as opposed to parameters contributing to the increase of SA such as rates of SA transport into PTC compartments. This indicates that in comparison to SA influx processes into PTC compartments, processes driving efflux and metabolism of SA may be less saturated. It is important to note that among all the transporter related $J_{\max}$ values applied here, $J_{\max(NPT1)}$ has the highest value, by a significant margin, that may explain why this value has a significant impact on PTC concentrations. $f_{u(p)SA}$ influences glomerular filtration and is a multiplicative factor in active transporter terms from renal blood to cellular compartments.

With and without the consideration of RAFs, the results of simulations with initial parameter values indicate that for all four individuals (young and healthy adult, elderly person at risk of CKD, elderly person with mild RI and elderly person with moderate RI) only the low, chronic therapeutic dose leads to proximal tubular concentrations below the previously set toxic concentration threshold of 0.09 mM. When RAFs are applied, predicted PTC concentrations for the mid and high exposure scenarios are twice to 20 times higher than PTC concentrations calculated without RAFs. Therefore, it would be beneficial to evaluate the validity of applied RAFs for SA transporter kinetics.

The results of scans for the chronic, low therapeutic dose show that for any value included in the scan, predicted proximal tubular concentrations are below 0.02 mM, i.e. significantly below

the hypothesised toxic threshold. Results of the scans for the two higher exposure scenarios re-emphasise that active transport $J_{max}$ values impact proximal tubular concentrations greatly and that interindividual variability in transporter expression may determine whether an adverse effect is experienced by an individual or not. As discussed in Appendix A.3, there are uncertainties underlying all active transporter $J_{max}$ values which is a limitation of this study. A reliable quantification of these uncertainties is crucial to the development of a robust model. It is interesting to note that for the two higher exposure scenarios the hypothesised toxicity threshold is exceeded at a $J_{\max(NPT1)}$ of approximately 390 µmol/min and higher for the elderly individuals at risk of CKD while the threshold is reached at approximately 600 µmol/min for the young and healthy adult. This discrepancy reflects the difference in transporter activity between the young and the three elderly individuals initially set due to the difference in the number of nephrons among them.

The results also emphasise that a decreased urinary pH, considered in the elderly with mild and moderate RI, has a substantial impact on proximal tubular cell concentrations. Physiologically, there are no significant differences between the elderly at risk of CKD and the elderly with mild RI (Table 7) apart from the pH. The difference in $GFR$ (60 vs. 50 mL/min) is minor and the flow rates of urinary filtrate through the tubular lumen ($FF_{PT}$, $FF_{HL}$, $FF_{DT}$) are not identified as greatly influencing PTC concentrations (see sensitivity analyses). Yet, for the two individuals with lower urinary pH, predicted PTC concentrations simulated with initial parameters are substantially higher at the two higher doses when compared with results for individuals with a urinary pH of 7.4 (Tables 9 and 10).

## 4. Discussion

This study offers a detailed description of the development of a mechanistic kidney model predicting the kinetics of SA and ASA. With regard to the first objective (i), this study shows how the mechanistic kidney model is embedded into a PBK model parameterised for ASA and SA and validated with data on the fractions of a dose excreted in urine as SA, ASA, SU and glucuronides. In accordance with the second objective (ii), an example is presented of how the PBK-coupled kidney model may be applied. For this, key parameters of this model, which is initially set up for a young and healthy adult, are adjusted to simulate kinetics of three virtual elderly individuals, one at risk of CKD, one with mild RI and one with moderate RI. For these four individuals three exposure scenarios are defined, including a chronic, low therapeutic dose, a chronic high therapeutic dose and acute intoxication. For these four individuals and three exposure scenarios defined, local sensitivity analyses are performed to understand which parameter values have the most impact on the predicted proximal tubular concentrations. To account for inter-individual variability and the uncertainty underlying parameter values (to some extent), parameters identified in the sensitivity analyses are changed over a predefined, biologically plausible ranges.

Overall, this study adds to the knowledgebase of mechanistic models related to kinetic processes and IVIVE approaches to increase the common understanding of nephrotoxicity induced by pharmaceutical compounds. All major kinetic factors (e.g. protein binding) and processes (i.e. glomerular filtration, urine flow, active and passive secretion and reabsorption) included in early models (Tang-Liu et al., 1983; Hall and Rowland, 1984; Komiya, 1986, 1987; Russel et al., 1987a; b; Mayer et al., 1988; Katayama et al., 1990) are taken into account in this model. Similar to the two most sophisticated mechanistic models to predict renal kinetics (Neuhoff et al., 2013; Huang and Isoherranen, 2018), the present model has the structure of a

nephron divided into segments illustrating the glomerulus, proximal and distal tubules, loop of Henle and collecting ducts. These segments are divided into vascular, cellular and luminal compartments. However, the model presented by Huang and Isoherranen (2018) has two segments for the loop of Henle and five for the collecting duct, whereas one and two, respectively, were used in the model presented here. These differ in the tubular flow rate entering each tubular segment and the tubular pH. Even though no references are given by Huang and Isoherranen (2018) to explain the choice of pH values, the values applied may be a good starting point to incorporate different pHs in each luminal compartment. Since luminal pH has an impact on the extent of passive reabsorption, one of the major kinetic processes in the kidney, it needs to be considered if the available data allow for it. Huang and Isoherranen (2018) address the issue of lacking factors to scale from *in vitro* to *in vivo* system activity, and propose a factor to scale the surface area of the *in vitro* systems to the real intrinsic permeability by considering microvilli expression. Their model is validated with data from 46 drugs, covering a wider applicability domain, whereas the model presented here is specific to SA.

In future studies it may be valuable to re-assess the volumes assigned to each compartment. As outlined in Appendix A.1, all compartment volumes of the mechanistic kidney model presented here add up to a total kidney volume of 280 mL. This volume has been used in PBK models generated in the past (Davies and Morris, 1993; Peters, 2008). In contrast, the volumes of all subsegments defined by Huang and Isoherranen (2018) add up to approximately one litre which exceeds the typical physiological volume of a kidney. Also, the volumes for the loop of Henle, used herein, may be considered high in comparison to volumes of the loop of Henle described qualitatively or semi-quantitatively in the literature; requiring further investigation in the future. The discrepancy between the approach to scale up volumes calculated from the external diameter, cell height and compartment length and the gross estimates of medullary compartments (discussed in Appendix A.1.4.2) may also indicate that these volumes need to be

re-assessed. Since the present investigation focusses on proximal tubular cell concentrations, potential inaccuracies in subsequent compartment volumes do not have a significant impact on the results of this study. Furthermore, the models presented by Neuhoff et al. (2013) and Huang and Isoherranen (2018) only incorporate renal metabolism and active transport processes at proximal tubular level. However, in this study metabolism is included on all levels starting from the proximal tubule since glucuronidation catalysing enzymes are reported to occur in latter tubular segments (Gaganis et al., 2007). Also, evidence indicates that active transport mechanisms exist in the renal medulla and collecting ducts (Madsen et al., 1988; Pearce et al., 2015). Furthermore, when validating the performance of the model with excretion data reported by Levy (1965), initial simulations show that active transport is needed to achieve the almost complete excretion of SA within 39 hours. In contrast to the model developed by Neuhoff et al. (2013), all data applied to generate this model are presented in this study.

This study contributes to the field of *in silico* toxicology since it is the first mechanistic model of the kidney which is embedded in a PBK model, where the data and ODEs used to generate both components of the models are comprehensively reported and publicly available. Additionally, in contrast to Huang and Isoherranen (2018), we amended certain physiological parameters of the model to simulate the physiology of two sensitive elderly individuals to address issues of variability.

The model presented here may be extended by making active transport processes from cellular to blood or luminal compartments only accessible to the fraction unbound. Due to a lack of information on protein binding of SA and metabolites in tubular cells, this component is not added to this model. However, it may be necessary to make active transport from cellular compartments only accessible to the fraction unbound in order to increase passive reabsorption of SA from cellular compartments. This process has currently a minor influence (particularly at a

pH of 7.4). Also, in order to reach the renal tissue/tubule level of the AOP proposed in Figure 1, reliable data explaining a quantitative relationship between an exposure level and acute tubular necrosis in humans are needed. However, the authors are not aware of these data being available to date. As soon as these become available or accessible, a quantitative dose-response relationship may be established between a dose or exposure scenario and necrosis observed at the renal tubular level.

There are several lessons learned from this study. The results of the sensitivity analyses performed for all individuals and exposure scenarios highlight that it is of major importance to use active transporter and metabolism data that are of good quality. Also, $f_{u(p)}$ may have a major impact on the predicted concentration in proximal tubules. The need for an accurate estimate of renal active transporter $V_{max}$ values has been highlighted previously (Felmlee et al., 2013). Since it is not necessarily straightforward to assess the quality of such data, using and comparing data from various sources helps to find an adequate value to inform the model (Min and Bae, 2017). Results presented here indicate that SA influx processes into PTC compartments may also be saturated at the chronic, high therapeutic dose leading to non-linear (zero-order) elimination processes. This implies that the elimination rate related to tubular secretion has reached its upper limit and is therefore no longer increasing proportionally to the concentration of SA in tubular blood compartments. When tubular secretion processes are fully saturated and plasma concentrations are increasing, glomerular filtration becomes the driver of renal excretion (van Ginneken and Russel, 1989). This is reflected in the results of the sensitivity analysis for the elderly individuals with decreased urinary pH (elderly with mild and moderate RI) which helps to establish confidence in the results generated.

Related to the quality of applied data, is adequate scaling of *in vitro* to *in vivo* data. The application of a relative expression factor (REF) or a RAF is proposed to scale from *in vitro* to *in vivo* transporter expression or activity, respectively, but such values are typically lacking (Neuhoff et al., 2013; Scotcher et al., 2016). Burt et al. (2016) and Mathialagan et al. (2017) proposed RAFs which are used here but their validity for the prediction of renal kinetics of SA still needs to be verified. The fact that glucuronidation $V_{max}$ values have to be increased in order to predict similar fractions of the dose excreted as glucuronides as observed in individuals indicates that a REF or RAF is needed to scale these $V_{max}$ values to *in vivo* activity. Overall, more human-based compound-specific data are needed to simulate kinetic processes. This holds in particular for active transport $J_{max}$ and $K_m$ data since most of these values used are generated with substances other than SA and/or in animal cell systems. IVIVE approaches to predict hepatic clearance are more advanced than IVIVE to simulate renal processes (Houston and Galetin, 2008; Obach, 2011; Chen et al., 2012; Scotcher et al., 2016; Min and Bae, 2017). The value of using certain extrapolation factors established for hepatic drug elimination for the prediction of renal drug elimination has not been assessed comprehensively but may hold potential to move the field of IVIVE for renal processes forward.

## Conflicts of Interest

No conflicts of interest.


## Funding

This paper was written as part of J Pletz's PhD project which is funded by the 2016 Liverpool John Moores University PhD Scholarship Scheme.

## 5. REFERENCES


Baker, R.E., Peña, J.-M., Jayamohan, J. and Jérusalem, A., (2018) Mechanistic models versus machine learning, a fight worth fighting for the biological community? *Biology Letters*, 145, pp.1–4.

Bernareggi, A. and Rowland, M., (1991) Physiologic modeling of cyclosporin kinetics in rat and man. *Journal of Pharmacokinetics and Biopharmaceutics*, 191, pp.21–50.

Bochner, F., Graham, G.G., Cham, B.E., Imhoff, D.M. and Haavisto, T.M., (1981) Salicylate metabolite kinetics after several salicylates. *Clinical Pharmacology and Therapeutics*, 302, pp.266–275.

Boroujerdi, M., (2015) *Pharmacokinetics and toxicokinetics*. Boca Raton: CRC Press, Taylor & Francis Group.

Burt, H.J., Neuhoff, S., Almond, L., Gaohua, L., Harwood, M.D., Jamei, M., Rostami-Hodjegan, A., Tucker, G.T. and Rowland-Yeo, K., (2016) Metformin and cimetidine: Physiologically based pharmacokinetic modelling to investigate transporter mediated drug–drug interactions. *European Journal of Pharmaceutical Sciences*, 88, pp.70–82.

Cha, S.H., Sekine, T., Kusuhara, H., Yu, E., Kim, J.Y., Kim, D.K., Sugiyama, Y., Kanai, Y. and Endou, H., (2000) Molecular cloning and characterization of multispecific organic anion transporter 4 expressed in the placenta. *Journal of Biological Chemistry*, 2756, pp.4507–4512.

Chen, Y., Jin, J.Y., Mukadam, S., Malhi, V. and Kenny, J.R., (2012) Application of IVIVE and PBPK modeling in prospective prediction of clinical pharmacokinetics: Strategy and approach during the drug discovery phase with four case studies. *Biopharmaceutics & Drug Disposition*, 332, pp.85–98.

Collins, A.J., Foley, R.N., Gilbertson, D.T. and Chen, S.C., (2015) United States Renal Data System public health surveillance of chronic kidney disease and end-stage renal disease. *Kidney International Supplements*, 51, pp.2–7.

Cook, J.D., Strauss, K.A., Caplan, Y.H., LoDico, C.P. and Bush, D.M., (2007) Urine pH: The effects of time and temperature after collection. *Journal of Analytical Toxicology*, 318, pp.486–496.

Cornish-Bowden, A., (2015) One hundred years of Michaelis–Menten kinetics. *Perspectives in Science*, 4, pp.3–9.

Davies, B. and Morris, T., (1993) Physiological parameters in laboratory animals and humans. *Pharmaceutical Research*, 107, pp.1093–1095.

Deguchi, T., Ohtsuki, S., Otagiri, M., Takanaga, H., Asaba, H., Mori, S. and Terasaki, T., (2002) Major role of organic anion transporter 3 in the transport of indoxyl sulfate in the kidney. *Kidney International*, 615, pp.1760–1768.

Delanaye, P., Schaeffner, E., Ebert, N., Cavalier, E., Mariat, C., Krzesinski, J.M. and Moranne, O., (2012) Normal reference values for glomerular filtration rate: What do we really know? *Nephrology Dialysis Transplantation*, 277, pp.2664–2672.

Denic, A., Lieske, J.C., Chakkera, H.A., Poggio, E.D., Alexander, M.P., Singh, P., Kremers, W.K., Lerman, L.O. and Rule, A.D., (2017) The substantial loss of nephrons in healthy human kidneys with aging. *Journal of the American Society of Nephrology : JASN*, 281, pp.313–320.

Derry, S., (2000) Risk of gastrointestinal haemorrhage with long term use of aspirin: meta-analysis. *BMJ*, 3217270, pp.1183–1187.

Drewe, W.C. and Surfraz, M.B., (2015) *Adverse outcome pathways for the nephrotoxicity of non-steroidal anti-inflammatory drugs (Poster)*. *SOT, 22-26 March 2015, San Diego, USA*.

Ducharme, M.P., (2016) Chapter 7: Drug elimination, clearance, and renal clearance. In: L.

Shargel and A.B.C. Yu, eds., *Applied Biopharmaceutics & Pharmacokinetics*, 7th ed. New York, USA: McGraw-Hill Education, pp.149–175.

Eaton, D.C. and Pooler, J.P., (2013) *Vander's Renal Physiology*. Eighth ed. New York: McGraw-Hill Medical.

Eirin, A., Lerman, A. and Lerman, L.O., (2017) The emerging role of mitochondrial targeting in kidney disease. In: *Handbook of Experimental Pharmacology*. pp.229–250.

El-Sheikh, A.A.K., van den Heuvel, J.J.M.W., Koenderink, J.B. and Russel, F.G.M., (2007) Interaction of nonsteroidal anti-inflammatory drugs with multidrug resistance protein (MRP) 2/ABCC2- and MRP4/ABCC4-mediated methotrexate transport. *Journal of Pharmacology and Experimental Therapeutics*, 3201, pp.229–235.

Emami Riedmaier, A., Burt, H., Abduljalil, K. and Neuhoff, S., (2016) More power to OATP1B1: An evaluation of sample size in pharmacogenetic studies using a rosuvastatin PBPK model for intestinal, hepatic, and renal transporter-mediated clearances. *Journal of Clinical Pharmacology*, 56S7, pp.S132–S142.

Eriksson, J.K., Neovius, M., Jacobson, S.H., Elinder, C.G. and Hylander, B., (2016) Healthcare costs in chronic kidney disease and renal replacement therapy: A population-based cohort study in Sweden. *BMJ Open*, 610, pp.1–9.

Feher, J., (2017) *Quantitative human physiology: An introduction*. Second ed. Cambridge, MA, USA: Academic Press/Elsevier.

Felmlee, M.A., Dave, R.A. and Morris, M.E., (2013) Mechanistic models describing active renal reabsorption and secretion: A simulation-based study. *The AAPS Journal*, 151, pp.278–287.

Felmlee, M.A., Wang, Q., Cui, D., Roiko, S.A. and Morris, M.E., (2010) Mechanistic toxicokinetic model for γ-hydroxybutyric acid: Inhibition of active renal reabsorption as a potential

therapeutic strategy. *The AAPS Journal*, 123, pp.407–416.

Fenton, R.A. and Praetorius, J., (2015) Chapter 2: Anatomy of the kidney. In: *Brenner and Rector's The Kidney, 2-Volume Set*, Tenth. Elsevier Inc., pp.42–80.

Furst, D.E., Tozer, T.N. and Melmon, K.L., (1979) Salicylate clearance, the resultant of protein binding and metabolism. *Clinical Pharmacology and Therapeutics*, 263, pp.380–389.

Gaganis, P., Miners, J.O., Brennan, J.S., Thomas, A. and Knights, K.M., (2007) Human renal cortical and medullary UDP-Glucuronosyltransferases (UGTs): Immunohistochemical localization of UGT2B7 and UGT1A enzymes and kinetic characterization of S-naproxen glucuronidation. *Journal of Pharmacology and Experimental Therapeutics*, 3232, pp.422–430.

van Ginneken, C.A.M. and Russel, F.G.M., (1989) Saturable pharmacokinetics in the renal excretion of drugs. *Clinical Pharmacokinetics*, 161, pp.38–54.

Guo, Y., Ni, J., Chen, S., Bai, M., Lin, J., Ding, G., Zhang, Y., Sun, P., Jia, Z., Huang, S., Yang, L. and Zhang, A., (2018) MicroRNA-709 mediates acute tubular injury through effects on mitochondrial function. *Journal of the American Society of Nephrology*, 292, pp.449–461.

Hall, S. and Rowland, M., (1984) Relationship between renal clearance, protein binding and urine flow for digitoxin, a compound of low clearance in the isolated perfused rat kidney. *Journal of Pharmacology and Experimental Therapeutics*, 2281, pp.174–179.

Hansson, L., Zanchetti, A., Carruthers, S.G., Dahlöf, B., Elmfeldt, D., Julius, S., Ménard, J., Rahn, K.H., Wedel, H. and Westerling, S., (1998) Effects of intensive blood-pressure lowering and low-dose aspirin in patients with hypertension: Principal results of the Hypertension Optimal Treatment (HOT) randomised trial. *The Lancet*, 351, pp.1755–1762.

Houston, J. and Galetin, A., (2008) Methods for predicting in vivo pharmacokinetics using data from in vitro assays. *Current Drug Metabolism*, 99, pp.940–951.

Hsu, V., Vieira, M.D.L.T., Zhao, P., Zhang, L., Zheng, J.H., Nordmark, A., Berglund, E.G., Giacomini, K.M. and Huang, S.M., (2014) Towards quantitation of the effects of renal impairment and probenecid inhibition on kidney uptake and efflux transporters, using physiologically based pharmacokinetic modelling and simulations. *Clinical Pharmacokinetics*, 533, pp.283–293.

Hsueh, C.H., Hsu, V., Zhao, P., Zhang, L., Giacomini, K.M. and Huang, S.M., (2018) PBPK modeling of the effect of reduced kidney function on the pharmacokinetics of drugs excreted renally by organic anion transporters. *Clinical Pharmacology and Therapeutics*, 1033, pp.485–492.

Huang, W. and Isoherranen, N., (2018) Development of a dynamic physiologically based mechanistic kidney model to predict renal clearance. *CPT: Pharmacometrics and Systems Pharmacology*, 79, pp.593–602.

Iharada, M., Miyaji, T., Fujimoto, T., Hiasa, M., Anzai, N., Omote, H. and Moriyama, Y., (2010) Type 1 sodium-dependent phosphate transporter (SLC17A1 protein) is a Cl-dependent urate exporter. *Journal of Biological Chemistry*, 28534, pp.26107–26113.

Ingalls, B.P. and Sauro, H.M., (2003) Sensitivity analysis of stoichiometric networks: An extension of metabolic control analysis to non-steady state trajectories. *Journal of Theoretical Biology*, 2221, pp.23–36.

Ishimoto, Y. and Inagi, R., (2016) Mitochondria: A therapeutic target in acute kidney injury. *Nephrology Dialysis Transplantation*, 317, pp.1062–1069.

Jakobsson, S. V and Cinti, D.L., (1973) Studies on the cytochrome P-450-containing mono-oxygenase system in human kidney cortex microsomes. *Journal of Pharmacology and Experimental Therapeutics*, 1852, pp.226–234.

Janků, I., (1993) Physiological modelling of renal drug clearance. *European Journal of Clinical Pharmacology*, 446, pp.513–519.

Katayama, K., Ohtani, H., Kawabe, T., Mizuno, H., Endoh, M., Kakemi, M. and Koizumi, T., (1990) Kinetic studies on drug disposition in rabbits. I. Renal excretion of iodopyracet and sulfamethizole. *Journal of Pharmacobio-Dynamics*, 132, pp.97–107.

Kerr, M., Bray, B., Medcalf, J., O'Donoghue, D.J. and Matthews, B., (2012) Estimating the financial cost of chronic kidney disease to the NHS in England. *Nephrology Dialysis Transplantation*, 27Suppl. 3, pp.iii73–iii80.

Khamdang, S., Takeda, M., Noshiro, R., Narikawa, S., Enomoto, A., Anzai, N., Piyachaturawat, P. and Endou, H., (2002) Interactions of human organic anion transporters and human organic cation transporters with nonsteroidal anti-inflammatory drugs. *Journal of Pharmacology and Experimental Therapeutics*, 3032, pp.534–539.

Knights, K.M. and Miners, J.O., (2010) Renal UDP-glucuronosyltransferases and the glucuronidation of xenobiotics and endogenous mediators. *Drug Metabolism Reviews*, 421, pp.60–70.

Knights, K.M., Spencer, S.M., Fallon, J.K., Chau, N., Smith, P.C. and Miners, J.O., (2016) Scaling factors for the in vitro-in vivo extrapolation (IV-IVE) of renal drug and xenobiotic glucuronidation clearance. *British Journal of Clinical Pharmacology*, 816, pp.1153–1164.

Komiya, I., (1986) Urine flow dependence of renal clearance and interrelation of renal reabsorption and physicochemical properties of drugs. *Drug Metabolism and Disposition*, 142, pp.239–245.

Komiya, I., (1987) Urine flow-dependence and interspecies variation of the renal reabsorption of sulfanilamide. *Journal of Pharmacobio-Dynamics*, 101, pp.1–7.

Kuehl, G.E., Bigler, J., Potter, J.D. and Lampe, J.W., (2006) Glucuronidation of the aspirin metabolite salicylic acid by expressed UDP-glucuronosyltransferases and human liver microsomes. *Drug Metabolism and Disposition*, 342, pp.199–202.

Lash, L.H., Putt, D.A. and Cai, H., (2008) Drug metabolism enzyme expression and activity in primary cultures of human proximal tubular cells. *Toxicology*, 2441, pp.56–65.

Levy, G., (1965) Pharmacokinetics of salicylate elimination in man. *Journal of Pharmaceutical Sciences*, 547, pp.959–67.

Levy, G. and Tsuchiya, T., (1972) Salicylate accumulation kinetics in man. *New England Journal of Medicine*, 2879, pp.430–432.

Lien, E.J., (1975) Chapter 3: Structure-absorption-distribution relationships: Significance for drug design. In: E.J. Ariëns, ed., *Drug design: Medicinal chemistry: A series of monographs, Volume V*. New York, USA: Acadmic Press, Inc., pp.81–132.

Lukacz, E.S., Sampselle, C., Gray, M., MacDiarmid, S., Rosenberg, M., Ellsworth, P. and Palmer, M.H., (2011) A healthy bladder: A consensus statement. *International Journal of Clinical Practice*, 6510, pp.1026–1036.

Madsen, K.M., Clapp, W.L. and Verlander, J.W., (1988) Structure and function of the inner medullary collecting duct. *Kidney International*, 344, pp.441–454.

Margaillan, G., Rouleau, M., Fallon, J.K., Caron, P., Villeneuve, L., Turcotte, V., Smith, P.C., Joy, M.S. and Guillemette, C., (2015) Quantitative profiling of human renal UDP-glucuronosyltransferases and glucuronidation activity: A comparison of normal and tumoral kidney tissues. *Drug Metabolism and Disposition*, 434, pp.611–619.

Martins, J., Kroo, I. and Alonso, J., (2000) An automated method for sensitivity analysis using complex variables. In: *38th Aerospace Sciences Meeting and Exhibit*. Reston, Virigina: American

Institute of Aeronautics and Astronautics, pp.1–12.

Martins, J.R.R.A., Sturdza, P. and Alonso, J.J., (2001) The connection between the complex-step derivative approximation and algorithmic differentiation. In: *39th Aerospace Sciences Meeting and Exhibit*. Reno, NV, USA: American Institute of Aeronautics and Astronautics, pp.1–11.

Mathialagan, S., Piotrowski, M.A., Tess, D.A., Feng, B., Litchfield, J. and Varma, M. V., (2017) Quantitative prediction of human renal clearance and drug-drug interactions of organic anion transporter substrates using in vitro transport data: A relative activity factor approach. *Drug Metabolism and Disposition*, 454, pp.409–417.

MathWorks, (2019) *ode15s*. [online] Available at: https://uk.mathworks.com/help/matlab/ref/ode15s.html [Accessed 28 Jan. 2019].

Matsson, P., Englund, G., Ahlin, G., Bergstrom, C.A.S., Norinder, U. and Artursson, P., (2007) A global drug inhibition pattern for the human ATP-binding cassette transporter breast cancer resistance protein (ABCG2). *Journal of Pharmacology and Experimental Therapeutics*, 3231, pp.19–30.

Mayer, J.M., Hall, S.D. and Rowland, M., (1988) Relationship between lipophilicity and tubular reabsorption for a series of 5-alkyl-5-ethylbarbituric acids in the isolated perfused rat kidney preparation. *Journal of Pharmaceutical Sciences*, 774, pp.359–364.

Mayo Clinic, (2019) *Daily aspirin therapy: Understand the benefits and risks*. [online] Available at: https://www.mayoclinic.org/diseases-conditions/heart-disease/in-depth/daily-aspirin-therapy/art-20046797 [Accessed 13 Jul. 2019].

MedicineNet, (2019) *Migraine a-z list: Aspirin*. [online] Available at: https://www.medicinenet.com/acetylsalicylic_acid/article.htm#which_drugs_or_supplements_interact_with_aspirin [Accessed 13 Jul. 2019].

Mehta, R.L., Pascual, M.T., Soroko, S., Savage, B.R., Himmelfarb, J., Ikizler, T.A., Paganini, E.P. and Chertow, G.M., (2004) Spectrum of acute renal failure in the intensive care unit: The PICARD experience. *Kidney International*, 664, pp.1613–1621.

Ménochet, K., Kenworthy, K.E., Houston, J.B. and Galetin, A., (2012a) Simultaneous assessment of uptake and metabolism in rat hepatocytes: A comprehensive mechanistic model. *Journal of Pharmacology and Experimental Therapeutics*, 3411, pp.2–15.

Ménochet, K., Kenworthy, K.E., Houston, J.B. and Galetin, A., (2012b) Use of mechanistic modeling to assess interindividual variability and interspecies differences in active uptake in human and rat hepatocytes. *Drug Metabolism and Disposition*, 409, pp.1744–1756.

Min, J.S. and Bae, S.K., (2017) Prediction of drug–drug interaction potential using physiologically based pharmacokinetic modeling. *Archives of Pharmacal Research*, 4012, pp.1356–1379.

Motojima, M., Hosokawa, A., Yamato, H., Muraki, T. and Yoshioka, T., (2002) Uraemic toxins induce proximal tubular injury via organic anion transporter 1-mediated uptake. *British Journal of Pharmacology*, 1352, pp.555–563.

Navar, L.G., (2009) Glomerular permeability: A never-ending saga. *American Journal of Physiology - Renal Physiology*, 2966, pp.F1266-1268.

Needs, C.J. and Brooks, P.M., (1985) Clinical pharmacokinetics of the salicylates. *Clinical Pharmacokinetics*, 102, pp.164–177.

Neuhoff, S., Artursson, P., Zamora, I. and Ungell, A.L., (2006) Impact of extracellular protein binding on passive and active drug transport across Caco-2 cells. *Pharmaceutical Research*, 232, pp.350–359.

Neuhoff, S., Gaohua, L., Burt, H., Jamei, M., Li, L., Tucker, G.T. and Rostami-Hodjegan, A.,

(2013) Accounting for transporters in renal clearance: Towards a mechanistic kidney model (Mech KiM). In: Y. Sugiyama and B. Steffansen, eds., *Transporters in drug development: Discovery, optimization, clinical study and regulation*. New York, USA: Springer, pp.155–177.

NHS, (2018) *Medicines A to Z: Low-dose aspirin*. [online] Available at: https://www.nhs.uk/medicines/low-dose-aspirin/ [Accessed 13 Jul. 2019].

Nozaki, Y., Kusuhara, H., Kondo, T., Iwaki, M., Shiroyanagi, Y., Nakayama, H., Horita, S., Nakazawa, H., Okano, T. and Sugiyama, Y., (2007) Species difference in the inhibitory effect of nonsteroidal anti-inflammatory drugs on the uptake of methotrexate by human kidney slices. *Journal of Pharmacology and Experimental Therapeutics*, 3223, pp.1162–1170.

Oates, C.J. and Mukherjee, S., (2012) Network inference and biological dynamics. *Annals of Applied Statistics*, 63, pp.1209–1235.

Obach, R.S., (2011) Predicting clearance in humans from in vitro data. *Current Topics in Medicinal Chemistry*, 114, pp.334–339.

Ohtsu, N., Anzai, N., Fukutomi, T., Kimura, T., Sakurai, H. and Endou, H., (2010) [Human renal urate transpoter URAT1 mediates the transport of salicylate] [article in Japanese]. *Nihon Jinzo Gakkai Shi*, [online] 524, pp.499–504. Available at: http://www.ncbi.nlm.nih.gov/pubmed/20560471.

Parvez, M.M., Shin, H.J., Jung, J.A. and Shin, J.G., (2017) Evaluation of para-aminosalicylic acid as a substrate of multiple solute carrier uptake transporters and possible drug interactions with nonsteroidal antiinflammatory drugs in vitro. *Antimicrobial Agents and Chemotherapy*, 615, pp.e02392-16.

Pearce, D., Soundararajan, R., Trimpert, C., Kashlan, O.B., Deen, P.M.T. and Kohan, D.E., (2015) Collecting duct principal cell transport processes and their regulation. *Clinical Journal of the*

*American Society of Nephrology : CJASN*, 101, pp.135–46.

Peters, S.A., (2008) Evaluation of a generic physiologically based pharmacokinetic model for lineshape analysis. *Clinical Pharmacokinetics*, 474, pp.261–275.

Petersen, P., Godtfredsen, J., Boysen, G., Andersen, E. and Andersen, B., (1989) Placebo-controlled, randomised trial of warfarin and aspirin for prevention of thromboembolic complications in chronic atrial fibrillation. *The Lancet*, 3338631, pp.175–179.

Pletz, J., Enoch, S.J., Jais, D.M., Mellor, C.L., Pawar, G., Firman, J.W., Madden, J.C., Webb, S.D., Tagliati, C.A. and Cronin, M.T.D., (2018) A critical review of adverse effects to the kidney: Mechanisms, data sources, and in silico tools to assist prediction. *Expert Opinion on Drug Metabolism and Toxicology*, 1412, pp.1225–1253.

Posada, M.M., Bacon, J.A., Schneck, K.B., Tirona, R.G., Kim, R.B., Higgins, J.W., Pak, Y.A., Hall, S.D. and Hillgren, K.M., (2015) Prediction of renal transporter mediated drug-drug interactions for pemetrexed using physiologically based pharmacokinetic modeling. *Drug Metabolism And Disposition*, 43, pp.325–334.

Roberts, M.A., Rumble, R.H., Wanwimolruk, S., Thomas, D. and Brooks, P.M., (1983) Pharmacokinetics of aspirin and salicylate in elderly subjects and in patients with alcoholic liver disease. *European Journal of Clinical Pharmacology*, 252, pp.253–261.

Rouiller, C., (1969) General anatomy and histology of the kidney. In: C. Rouiller and A.F. Muller, eds., *The kidney: Morphology, biochemistry, physiology*, First. New York, USA: Elsevier, pp.61–156.

Rowland, M., (1984) Protein binding and drug clearance. *Clinical Pharmacokinetics*, 91, pp.10–17.

Russel, F.G.M., Wouterse, A.C. and van Ginneken, C.A.M., (1987a) Physiologically based

pharmacokinetic model for the renal clearance of phenolsulfonphthalein and the interaction with probenecid and salicyluric acid in the dog. *Journal of Pharmacokinetics and Biopharmaceutics*, 154, pp.349–368.

Russel, F.G.M., Wouterse, A.C. and van Ginneken, C.A.M., (1987b) Physiologically based pharmacokinetic model for the renal clearance of salicyluric acid and the interaction with phenolsulfonphthalein in the dog. *Drug Metabolism and Disposition*, 155, pp.695–701.

Scotcher, D., Jones, C., Posada, M., Galetin, A. and Rostami-Hodjegan, A., (2016) Key to opening kidney for in vitro-in vivo extrapolation entrance in health and disease: Part II: Mechanistic models and in vitro-in vivo extrapolation. *The AAPS Journal*, 185, pp.1082–1094.

Scotcher, D., Jones, C.R., Galetin, A. and Rostami-Hodjegan, A., (2017) Delineating the role of various factors in renal disposition of digoxin through application of physiologically based kidney model to renal impairment populations. *Journal of Pharmacology and Experimental Therapeutics*, 3603, pp.484–495.

Sedykh, A., Fourches, D., Duan, J., Hucke, O., Garneau, M., Zhu, H., Bonneau, P. and Tropsha, A., (2013) Human intestinal transporter database: QSAR modeling and virtual profiling of drug uptake, efflux and interactions. *Pharmaceutical Research*, 304, pp.996–1007.

Sekine, T., Tsuda, M., Apiwattanakul, N., Nakajima, N., Kanai, Y., Endou, H. and Cha, S.H., (1998) Identification of multispecific organic anion transporter 2 expressed predominantly in the liver. *FEBS Letters*, 4292, pp.179–182.

Shen, H., Liu, T., Morse, B.L., Zhao, Y., Zhang, Y., Qiu, X., Chen, C., Lewin, A.C., Wang, X.T., Liu, G., Christopher, L.J., Marathe, P. and Lai, Y., (2015) Characterization of organic anion transporter 2 (SLC22A7): A highly efficient transporter for creatinine and species-dependent renal tubular expression. *Drug Metabolism and Disposition*, 437, pp.984–993.

Takeda, M., Khamdang, S., Narikawa, S., Kimura, H., Hosoyamada, M., Cha, S.H., Sekine, T. and Endou, H., (2002) Characterization of methotrexate transport and its drug interactions with human organic anion transporters. *Journal of Pharmacology and Experimental Therapeutics*, 3022, pp.666–671.

Tang-Liu, D.D.-S., Tozer, T.N. and Riegelman, S., (1983) Dependence of renal clearance on urine flow: A mathematical model and its application. *Journal of Pharmaceutical Sciences*, 722, pp.154–158.

The Salt Collaborative Group, (1991) Swedish Aspirin Low-dose Trial (SALT) of 75 mg aspirin as secondary prophylaxis after cerebrovascular ischaemic events. *The Lancet*, 3388779, pp.1345–1349.

Tojo, A. and Kinugasa, S., (2012) Mechanisms of glomerular albumin filtration and tubular reabsorption. *International Journal of Nephrology*, 2012, pp.1–9, Article ID 481520.

Tucker, G.T., (1981) Measurement of the renal clearance of drugs. *British Journal of Clinical Pharmacology*, 12, pp.761–770.

Uchino, S., Kellum, J.A., Bellomo, R., Doig, G.S., Morimatsu, H., Morgera, S., Schetz, M., Tan, I., Bouman, C., Macedo, E., Gibney, N., Tolwani, A. and Ronco, C., (2005) Acute renal failure in critically ill patients: A multinational, multicenter study. *JAMA*, 2947, pp.813–818.

United States Renal Data System (USRDS), (2017) Chapter 1: CKD in the general population. *American Journal of Kidney Diseases*, 693, pp.S33–S52.

Weiner, I.M., Washington, J.A. and Mudge, G.H., (1960) On the mechanism of action of probenecid on renal tubular secretion. *Bulletin of the John Hopkins Hospital*, 106, pp.333–346.

Weinstein, J.R. and Anderson, S., (2010) The aging kidney: Physiological changes. *Advances in Chronic Kidney Disease*, 174, pp.302–307.

Wolff, N.A., Burckhardt, B.C., Burckhardt, G., Oellerich, M. and Armstrong, V.W., (2007) Mycophenolic acid (MPA) and its glucuronide metabolites interact with transport systems responsible for excretion of organic anions in the basolateral membrane of the human kidney. *Nephrology Dialysis Transplantation*, 229, pp.2497–2503.

Wood, D.M., Dargan, P.I. and Jones, A.L., (2005) Measuring plasma salicylate concentrations in all patients with drug overdose or altered consciousness: Is it necessary? *Emergency Medicine Journal*, 226, pp.401–403.

Yang, C.H., Glover, K.P. and Han, X., (2010) Characterization of cellular uptake of perfluorooctanoate via organic anion-transporting polypeptide 1A2, organic anion transporter 4, and urate transporter 1 for their potential roles in mediating human renal reabsorption of perfluorocarboxylates. *Toxicological Sciences*, 1172, pp.294–302.

You, K., (1983) Salicylate and mitochondrial injury in Reye's syndrome. *Science*, 221July, pp.163–165.

Zhang, L., Wang M and Wang, H., (2005) Acute renal failure in chronic kidney disease - clinical and pathological analysis of 104 cases. *Clinical Nephrology*, 635, pp.346–350.